Detailed Investigation and Performance Improvement of the Dynamic Behavior of Grid-Connected DFIG-Based Wind Turbines under LVRT Conditions

Alsmadi, Yazan M.; Xu, Longya; Blaabjerg, Frede; Ortega, Alejandro J.Pina; Abdelaziz, Almoataz Y.; Wang, Aimeng; Albataineh, Zaid

Published in:
IEEE Transactions on Industry Applications

DOI (link to publication from Publisher):
10.1109/TIA.2018.2835401

Publication date:
2018

Document Version
Accepted author manuscript, peer reviewed version

This article has been accepted for publication in a future issue of this journal, but has not been fully edited. Content may change prior to final publication. Citation information: DOI 10.1109/TIA.2018.2835401, IEEE Transactions on Industry Applications

Detailed Investigation and Performance Improvement of the Dynamic Behavior of Grid-Connected DFIG-Based Wind Turbines under LVRT Conditions

Yazan M. Alsmadi[1], Longya Xu[2], Frede Blaabjerg[3], Alejandro Pina Ortega[4], Almoataz Y. Abdelaziz[5], Aimeng Wang[6] and Zaid Albataineh[7]

[1]Department of Electrical Engineering, Jordan University of Science and Technology, Irbid 22110, Jordan
[2]Department of Electrical and Computer Engineering, The Ohio State University, Columbus, OH, U.S.A
[3]Department of Energy Technology, Aalborg University, DK-9220 Aalborg East, Denmark
[4]Research Design and Development (RDD), Dyson Ltd, Malmesbury, SN 16 0RP, United Kingdom
[5]Electrical Power and Machines Department, Ain Shams University, Cairo 11517, Egypt
[6]State Key Laboratory of Alternate Electrical Power Systems, North China Electric Power University, Baoding 071003, China
[7]Department of Electronics Engineering, Yarmouk University, Irbid 21163, Jordan

***Abstract*— Power generation and grid stability have become key issues in the last decade. The high penetration of large capacity wind generation into the electric power grid has led to serious concerns about their influence on the dynamic behavior of power systems. The Low-Voltage Ride-Through (LVRT) capability of wind turbines during grid faults is one of the core requirements to ensure stability in the power grid during transient conditions. The doubly-fed induction generators (DFIGs) offer several advantages when utilized in wind turbines, but discussions about their LVRT capabilities are limited. This paper presents a comprehensive study of the LVRT of grid-connected DFIG-based wind turbines. It provides a detailed investigation of the transient characteristics and the dynamic behavior of DFIGs during symmetrical and asymmetrical grid voltage sags. A detailed theoretical study supported by computer simulations is provided. This paper also provides a new rotor-side control scheme for DFIG-based wind turbines to enhance its LVRT capability during severe grid voltage sags. The proposed control strategy focuses on mitigating the rotor-side voltage and current shock during abnormal grid conditions, without any additional cost or reliability issues. As a result, the DFIG performance is improved and utility company standards are fulfilled. Computer simulations are used to verify the expanded ride-through capability of the novel strategy and its effective performance compared to the conventional control schemes.**

***Index Terms*— Wind power generation, Doubly-fed induction generator (DFIG), Grid fault, Low-Voltage Ride-Through (LVRT), Power converters.**

I. INTRODUCTION

In recent years, there has been a huge increase in global demand for energy as a result of not only industrial development, but also population growth. Consequently, the rise in consumption of traditional fossil fuels has led to many serious problems such as energy shortages, pollution, global warming, the shortfall of traditional fossil energy sources, and energy insecurity. These factors are driving the development of renewable energy technologies, which are considered an essential part of a well-balanced energy portfolio [1]-[4]. Wind power is thought to be the most promising near-term alternative energy. As renewable energy sources grow in popularity, wind power is currently one of the fastest growing renewable sources of electrical energy [3], [4]. More than 54 GW of wind power was installed in 2016, and it is expected to be higher in 2017 [1], [2].

With the increased presence of wind energy in the power system over the last decade, a serious concern about its influence on the dynamic behavior of the electric power network has arisen [4]-[6]. Therefore, it becomes essential that grid-connected wind turbines behave similarly to conventional power plants and support the power network during normal and abnormal grid conditions. This has required many countries to develop specific grid codes for operation and grid integration of wind turbines. Among these grid codes, two main issues are of special concern for engineers in the area of power and energy: a) active and reactive power control in normal conditions, and b) Low-Voltage Ride-Through (LVRT) capability during grid faults, or more succinctly, Fault Ride-Through (FRT) capability [4], [6].

In addition to the progress made in the creation of adequate grid codes for the proper utilization of wind energy, a significant improvement has been achieved in the design and implementation of robust energy conversion systems that efficiently transform wind energy. The Doubly-Fed Induction Generator (DFIG)-based wind turbine has become one of the most favorable choices in wind power generation. This is due to the prominent advantages that it has compared to the other energy conversion systems that are currently available in the market. However, the dynamic response of the DFIG to grid voltage transients is the most serious problem [7]-[9].

DFIG-based wind turbines are sensitive to voltage sags during grid faults. This is due to the partial-scale back-back power converters that connect the rotor of the generator to the power grid. Faults in the power system, even far away from the location of the turbine, can cause an abrupt drop of the grid voltage which leads to an over-voltage in the DC bus and an over-current in the rotor circuit of the generator [10]-[13]. Without any protection scheme, this can lead to power converter damage. Moreover, it may also increase the speed of the turbine above the rated limits if not properly designed,

This article has been accepted for publication in a future issue of this journal, but has not been fully edited. Content may change prior to final publication. Citation information: DOI 10.1109/TIA.2018.2835401, IEEE Transactions on Industry Applications

which will threaten the safe operation of the turbine [10]-[16]. Therefore, the LVRT ability of DFIG-based wind turbines during grid faults are intensively investigated in order to provide proper solutions that can protect the turbine during abnormal conditions on the grid.

The objective of this paper is to provide a comprehensive and simplified study of the dynamic behavior of grid-connected DFIG-based wind turbines under LVRT conditions. Detailed analysis of the LVRT of DFIGs, including the voltage sag profile, transient characteristics and the behavior of the DFIG at the moments of voltage sag, as well as the subsequent voltage recovery, is investigated. A simplified dynamic model of the DFIG is used to investigate the performance of the wind energy generation system under the influence of symmetrical and asymmetrical grid faults.

This paper also provides a detailed description of the most cited and commonly used LVRT solutions by improving the Rotor-Side Converter (RSC) control strategies (active methods). It describes the basic operation principle, advantages and disadvantages of each proposed solution.

In the end, a new rotor-side control scheme for DFIG-based wind turbines is developed to enhance its LVRT capability during severe grid voltage sags. The proposed control strategy focuses on mitigating the rotor-side voltage and current shock during abnormal grid conditions, without any additional cost or reliability issues. As a result, the DFIG performance is improved and the utility company standards are fulfilled. Computer simulations are used to verify the expanded ride-through capability of the novel strategy and its effective performance compared to the conventional control schemes.

The paper is organized as follows: Section II provides a detailed description of the DFIG-based wind power generation system. This includes the DFIG's dynamic model and a comprehensive analysis of its complicated dynamic behavior during different types of grid faults. Section III describes the LVRT grid code of DFIGs. This includes the LVRT characteristic and major LVRT technologies. It also summarizes the most cited and commonly used LVRT solutions for DFIG by improving the RSC control strategies. Section IV develops a new rotor-side control scheme for DFIGs to enhance their LVRT capability during severe grid voltage sags. Conclusions are presented in section V.

II. DFIG-Based Wind Power Generation System

At present, commercial wind turbines mix and match a variety of innovative concepts with proven technologies for both generators and power electronics. Different wind turbine configurations can be obtained by combining an induction or synchronous generator with fully or partially rated power converters [10], [17], [18]. The state-of-the-art variable speed wind turbine generators are categorized by two major types: Permanent Magnet Synchronous Generators (PMSGs)-based wind turbines with fully rated power converters and DFIG-based wind turbines with partially rated power converters, as shown in Fig. 1 and Fig. 2, respectively.

The DFIG is a perfect solution for systems with limited variable-speed range, e.g. ±30% of the synchronous speed. The reason is that the power electronic converter has to handle a fraction (20–30%) of the total generated power compared to the direct drive PMSG-based wind turbines. As a result, the equipment cost and operational losses of the power converter can be significantly reduced compared to a system where the converter has to handle the total generated power [8], [17].

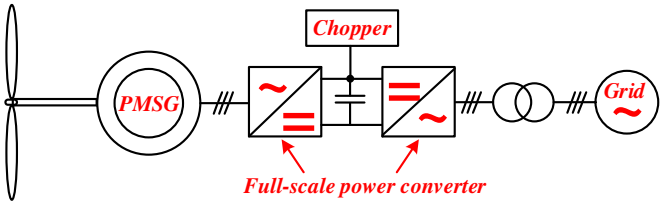

Fig. 1. Wind turbine configuration of the PMSG-based wind turbine with fully rated back-back converters.

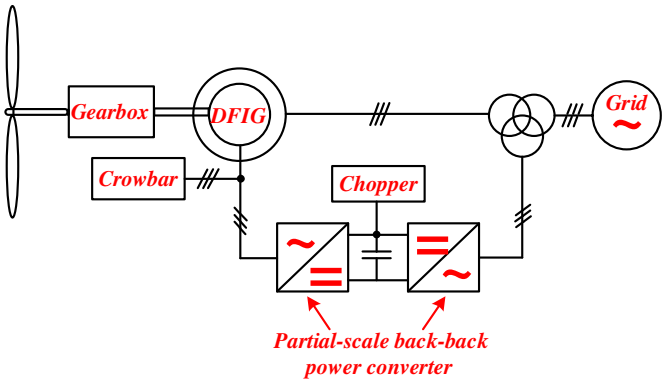

Fig. 2. Wind turbine configuration of the DFIG-based wind turbine with partially rated back-back power converters and a gearbox.

The back-to-back power converter in the DFIG system consists of two converters, i.e., a Rotor-Side Converter (RSC) and a Grid-Side Converter (GSC), which are connected back-to-back by a dc-link. Between the two converters, a dc-link capacitor is placed as energy storage in order to limit voltage variations (or ripple) in the dc-link voltage. With the RSC, it is possible to control the torque, the speed of DFIG as well as the active and reactive powers at the stator terminals. The main objective for the GSC is to keep the dc-link voltage constant. It can also be used to control the reactive power flowing from or to the power grid [8], [17]-[21].

DC-link over-voltages may arise as a result of wind turbine response to unbalanced grid faults or load shedding situations [10], [12]-[14]. In this case, the direction of the power flow is reversed and the current flows to the dc-link. Therefore, the DC-link voltage must be limited to its rated value. This can be achieved by using a DC-side crowbar circuit that consists of a chopper and a resistor connected across the DC–link of the converters, as shown in Fig. 2. This configuration can limit the DC bus voltage from exceeding the safe operating range by short-circuiting the dc-link through the chopper resistors.

A. Dynamic Modeling of DFIG

The operating principle of the variable speed DFIG can be conveniently analyzed by the classical rotating field theory with the well-known *Park* and *Clarke* transformations [21], [22]. Since the DFIG can be regarded as a traditional induction generator with non-zero rotor voltage, its dynamic equivalent

This article has been accepted for publication in a future issue of this journal, but has not been fully edited. Content may change prior to final publication. Citation information: DOI 10.1109/TIA.2018.2835401, IEEE Transactions on Industry Applications

circuit in the *dq*-synchronous reference frame can be modeled as shown in Fig. 3.

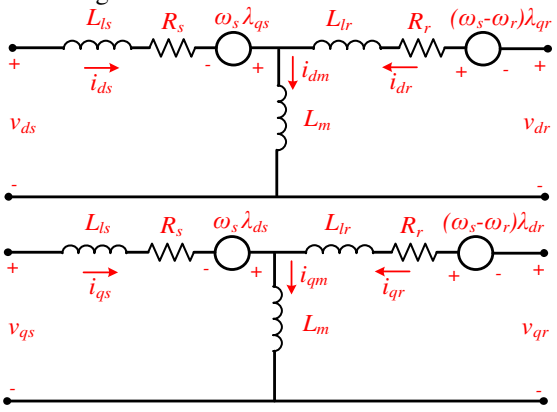

Fig. 3. Equivalent circuit of the DFIG in the *dq*-synchronous reference frame

The full-order dynamic model of DFIG in the synchronous rotating reference frame can be described as given [21]-[23]:

$$\begin{cases} v_{ds} = r_s i_{ds} + \dfrac{d\lambda_{ds}}{dt} - \omega_s\lambda_{qs} \\ v_{qs} = r_s i_{qs} + \dfrac{d\lambda_{qs}}{dt} + \omega_s\lambda_{ds} \\ v_{dr} = r_r i_{dr} + \dfrac{d\lambda_{dr}}{dt} - (\omega_s-\omega_r)\lambda_{qs} \\ v_{qr} = r_r i_{qr} + \dfrac{d\lambda_{qr}}{dt} - (\omega_s-\omega_r)\lambda_{dr} \\ \lambda_{ds} = L_s i_{ds} + L_m i_{dr} \\ \lambda_{qs} = L_s i_{qs} + L_m i_{qr} \\ \lambda_{dr} = L_r i_{dr} + L_m i_{ds} \\ \lambda_{qr} = L_r i_{qr} + L_m i_{qs} \\ L_s = L_{ls} + L_m \\ L_r = L_{lr} + L_m \end{cases} \quad (1)$$

where the subscripts "*s*" and "*r*" represent the stator and rotor sides, r_s *and* r_r are resistances of the stator and rotor windings, L_m is the magnetizing inductance, L_{ls} and L_{lr} are the stator and rotor leakage inductances, λ_s and λ_r are the stator and rotor magnetic flux linkages, v_s and i_s are the stator voltage and current, v_r and i_r are the rotor voltage and current, ω_s is the electrical angular velocity of the synchronous reference frame, and ω_r is the electrical angular velocity of the rotor.

It is shown in [23] that several simplifications can be made to the system given in (1) since the DFIG-based wind turbine is considered to be part of an electrical system that includes other components such as the power converters and electrical networks.

The objective of the following analysis is to find a direct relationship between the stator and rotor voltages, currents and flux linkages. It will be assumed that the RSC acts as a current source where the objective of the DFIG is to supply a certain power to the grid by controlling the injected rotor currents.

First, the stator flux-oriented synchronous reference frame, where the *q*-axis is aligned to the positive-sequence stator flux, is applied to the DFIG full-order model given in (1). Neglecting the stator resistance, the rotor voltage equations can be expressed as [24]:

$$v_{dr} = \left(r_r + \sigma L_r \frac{d}{dt}\right) i_{dr} - (\omega_s - \omega_r)\sigma L_r i_{qr} + \frac{L_m}{L_s}(v_{ds}) \quad (2)$$

$$v_{qr} = (\omega_s - \omega_r)\sigma L_r i_{dr} + \left(r_r + \sigma L_r \frac{d}{dt}\right) i_{qr} + \frac{L_m}{L_s}(v_{qs} - \omega_r\lambda_{ds}) \quad (3)$$

where $\sigma = 1 - \frac{L_m^2}{L_s L_r}$. The previous equations can also be written in a matrix format as:

$$\begin{bmatrix} v_{dr} \\ v_{qr} \end{bmatrix} = \begin{bmatrix} r_r + \sigma L_r \dfrac{d}{dt} & -(\omega_s - \omega_r)\sigma L_r \\ (\omega_s - \omega_r)\sigma L_r & \left(r_r + \sigma L_r \dfrac{d}{dt}\right) \end{bmatrix} \begin{bmatrix} i_{dr} \\ i_{qr} \end{bmatrix} + \frac{L_m}{L_s}\begin{bmatrix} v_{ds} \\ v_{qs} - \omega_r\lambda_{ds} \end{bmatrix} \quad (4)$$

Equation (4) holds for both steady-state and dynamic conditions. It provides a direct relationship between the instantaneous values of the stator and rotor *dq*-voltages to the *dq* rotor currents. The stator flux is normally estimated by integrating the stator voltage. During steady-state conditions, with neglecting r_r and L_r and approximating $\frac{L_m}{L_s} \approx 1$, the RSC AC-side output voltage is approximately sV_s (referred to the rotor side), where s is the slip and V_s is the magnitude of the steady-state stator voltage. Since the slip of the DFIG is normally limited between -0.3 and 0.3, then according to equation (4), the RSC needs to be able to output at least 30% of the stator voltage and thereby provide a minimum of 30% of the generator ratings. A specified safety margin is normally required.

If a sudden voltage sag happens at the stator terminals, the necessary rotor terminal voltage could be directly determined from (4) such that the rotor current will not be affected and remains unchanged. However, since the RSC rating is limited and cannot generate the necessary rotor voltage, a large transient in the rotor current will appear during grid voltage sags.

Considering that the DFIG fifth-order model, given by (1), is linear, and applying the Laplace transform, the *dq*-stator currents in the synchronous reference frame can be expressed as [23]-[25]:

$$i_{ds} = \frac{1}{L_s}\frac{\omega_s}{s^2 + 2\frac{1}{\tau_s}s + \omega_s^2} v_{qs} - \frac{L_m}{L_s} i_{dr} \quad (5)$$

$$i_{qs} = \frac{1}{L_s}\frac{s + {}^1\!/_{\tau_s}}{s^2 + 2\frac{1}{\tau_s}s + \omega_s^2} v_{qs} - \frac{L_m}{L_s} i_{qr} \quad (6)$$

where τ_s is the stator time constant. Equations (5) and (6) directly relate the stator current to the stator voltage, clamped by the grid voltage, and the rotor current, controlled by the

This article has been accepted for publication in a future issue of this journal, but has not been fully edited. Content may change prior to final publication. Citation information: DOI 10.1109/TIA.2018.2835401, IEEE Transactions on Industry Applications

RSC. During a voltage sag, when the rotor current is kept constant, stator current starts to oscillate with stator frequency (ω_s) and oscillation damping depends on the stator time constant (τ_s). During asymmetrical faults, a negative sequence will appear and also force oscillations but with a frequency equal to ($2\omega_s$) [11], [23], [25], [26].

It is also demonstrated in [26] that the direct relationship between stator flux linkage, stator voltage and rotor current, using the stator voltage-oriented synchronous reference frame ($v_{qs} = 0$ and $v_s = v_{ds}$), can be derived as:

$$\lambda_{ds} = \frac{s + 1/\tau_s}{s^2 + 2\frac{1}{\tau_s}s + \omega_s^2} v_{ds} - \frac{L_m/\tau_s(s + 1/\tau_s)}{s^2 + 2\frac{1}{\tau_s}s + \omega_s^2} i_{dr} \quad (7)$$

$$\lambda_{qs} = \frac{-\omega_s}{s^2 + 2\frac{1}{\tau_s}s + \omega_s^2} v_{ds} - \frac{L_m/\tau_s(s + 1/\tau_s)}{s^2 + 2\frac{1}{\tau_s}s + \omega_s^2} i_{qr} \quad (8)$$

Equations (7) and (8) show that stator flux linkage depends on stator voltage and rotor current, explaining the behavior of the DFIG during grid faults. If a voltage sag happens at the stator terminals and rotor current is kept constant, the stator flux starts to oscillate with the stator frequency (ω_s) and the oscillation damping depends on the stator time constant (τ_s). During asymmetrical faults, a negative sequence will appear and also force oscillations but with a frequency equal to ($2\omega_s$) [23], [26], [27].

B. Transient Analysis of the DFIG Magnetic Flux during Grid Faults

Symmetrical Faults

At steady state, the stator flux is a vector that rotates at synchronous speed with respect to stator and has a constant amplitude proportional to the grid voltage [11]-[15]. Reactive current excites the magnetic field, which sets up the air gap flux required for the reactive power flow between the stator and the rotor as well as active power flow between the mechanical and electrical ports. Any voltage sag at the stator terminals causes fluctuations in the stator flux. This leads to a large transient current in the rotor circuit [13], [27]-[29].

Fig. 4 illustrates the dynamic behavior of the stator flux during a three-phase partial voltage sag. During normal operating conditions, the flux vector rotates along the outer red circle that is labeled as AC flux pre-fault trajectory. Assuming that a three-phase grid voltage sag happens at the moment corresponding to point A, the stator flux vector is unable to maintain the same magnitude as the magnitude prior to the fault, because the magnetic field cannot be changed instantaneously. As a result, the flux vector is split into two components: the frozen DC flux component OO', and the AC synchronous rotating component AO'. Just after the fault, the origin of the synchronously rotating flux vector offsets the old one by a DC flux vector OO', which has a passive nature and decays gradually along the green line. Lastly at Point B, the transient caused by the voltage sag ends with the AC flux vector rotating along the smaller inner red circle.

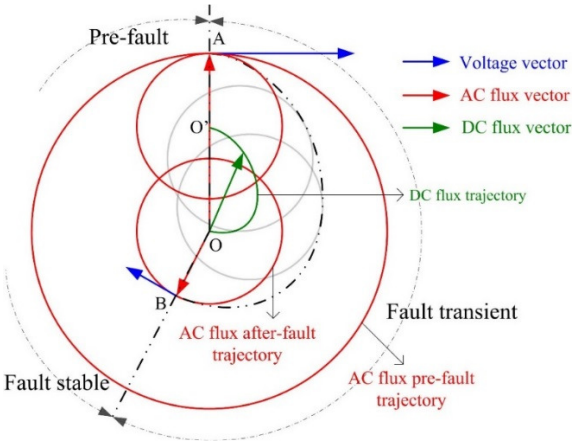

Fig. 4. Stator flux (λ_s) trajectory during three-phase to ground grid voltage sag.

Fig. 5 shows the simulated three-phase stator flux trajectory of a 1.5 MW DFIG under the influence of a partial three-phase grid voltage sag (step change). Parameters of the simulated DFIG system are listed in Table 1 of the appendix. The depth of the voltage sag is 70%. At the moment of the sag ($t = 5$ sec), the stator flux is divided into two components: one component rotating synchronously and proportional to the remaining grid voltage during the fault, and a second DC (natural) component fixed with the stator and decays exponentially to zero based on the stator time constant. Furthermore, a transient recovery is considered an abrupt change in the stator voltage and it induces a DC component in the magnetic flux. The phase difference between the sag and recovery moments is the only factor that determines whether the current and magnetic flux DC components aggravate or mitigate the transients. Note that the fault duration was selected to be 1 sec for illustration only. The fault is normally cleared within 1.5-2 cycles. Furthermore, the stator time constant was adjusted by increasing the resistance of the stator windings. The goal is to accelerate the decay of the DC component in order to perfectly illustrate the behavior of the stator flux linkage during the grid voltage sag. However, changing the resistance of the stator winding is a less favored approach because the resistors used for the current decay handle high energy and power and will typically be bulky. In addition, the cutting-in and cutting out of resistors will introduce additional transient into the system [13], [28], [29].

Fig. 6, Fig. 7, and Fig. 8 show 2-D and 3-D plots of the simulated dq and $\alpha\beta$ stator flux linkage components during a three-phase partial voltage sag (step change), respectively. The effect of the DC component on the stator flux trajectory is clear from the figures, especially during the recovery time. It can be seen that the centers of the two trajectories (circles) during the fault and the recovery are far away from each other due to the large DC flux component that was generated as a result of the fault and recovery. Without the effect of the generated DC component, the two circles should have the same center with different radii.

This article has been accepted for publication in a future issue of this journal, but has not been fully edited. Content may change prior to final publication. Citation information: DOI 10.1109/TIA.2018.2835401, IEEE Transactions on Industry Applications

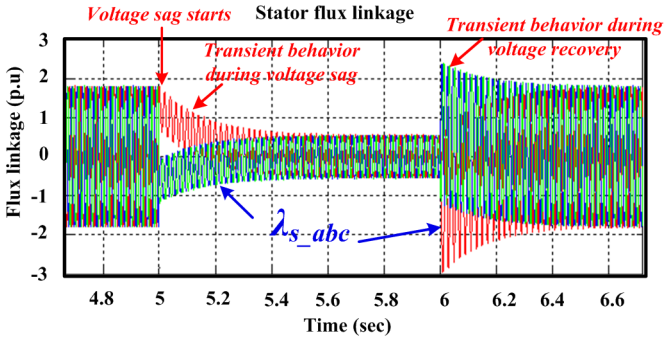

Fig. 5. Three-phase stator flux ($\lambda_{s\text{-}abc}$) of a 1.5 MW DFIG during a three-phase partial voltage sag.

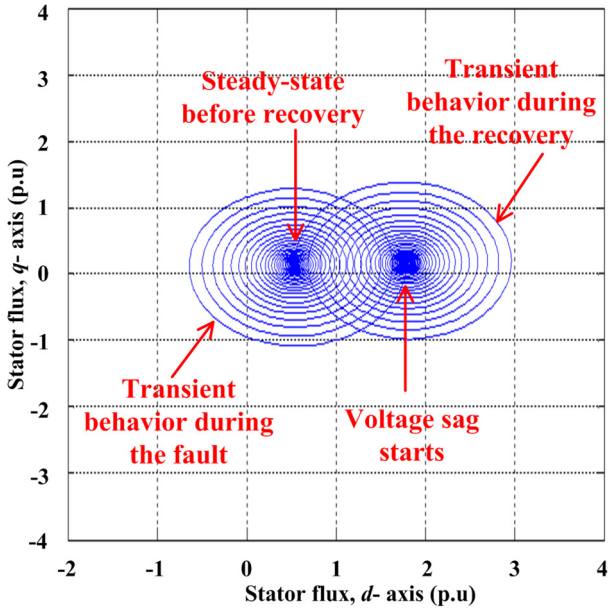

Fig. 6. 2-D plot of the dq stator flux linkage components before, during and after a three-phase voltage sag.

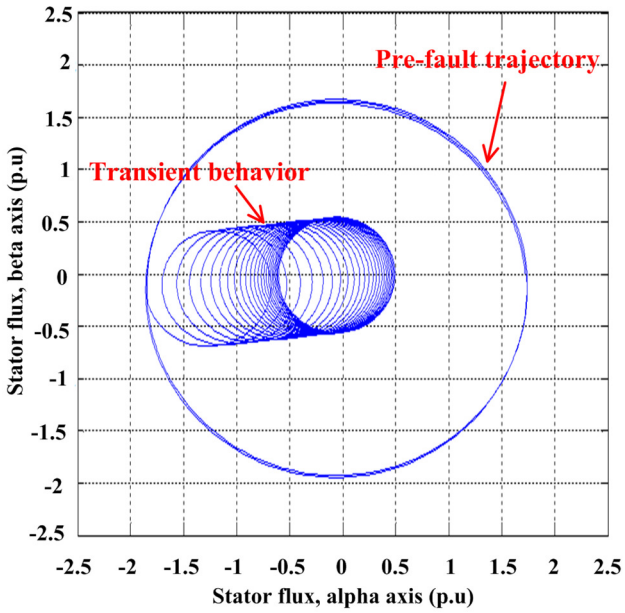

Fig. 7. 2-D plot of the $\alpha\beta$ stator flux linkage components before, during and after a three-phase voltage sag.

Flux variation will be also associated with energy flow during voltage sag. The AC magnetic field, excited by AC currents, supports the normal active power flow from mechanical to electrical ports for generating operation. At the moment of fault, the transient DC flux component is induced, supported by the DC excitation current, and the DC magnetic flux also participates in the active and reactive power transfer, if it is properly controlled.

Power flow before and after the voltage sag can be illustrated by Fig. 9. As shown, the AC magnetic field transfers all the active energy before fault. After the voltage sag, the AC related energy flow is reduced. However, the transient DC magnetic field is able to transfer additional energy. Therefore, if both the AC and DC current components corresponding to the respective magnetic fields are controlled, the system can survive any voltage fault. The protection includes prevention of large surge current in the rotor circuit as well as sudden torque pulsations on the rotor shaft.

Fig. 10 shows the simulated rotor voltage during a three-phase grid voltage sag. The DFIG is operated in the super-synchronous speed mode with slip $s = -33\%$. In this test, the fault duration is 0.31 sec. Furthermore, τ_s is kept constant and it is not adjusted by changing the resistance of the stator windings. The rotor current is tightly controlled to track the command. The RSC has to generate the necessary rotor terminal voltage such that the rotor current will not be affected and remains unchanged. As it can be seen, at the instant of the fault, the rotor voltage jumps from a value of 500 V to almost 1000 V, which is about two times the pre-fault value. The situation is more dangerous during the recovery time when the rotor voltage jumps to a value close to 2500 V. These large transient values of the rotor voltage exceed the RSC voltage limit, which is 1000 V, particularly during the fault recovery time.

The reaction of the DFIG rotor voltage, shown in Fig. 10, is due to the fact that the stator DC flux component, during the three-phase voltage sag, will induce a voltage component in the rotor circuit, which is given by [10]:

$$\vec{v}_{rn}^{\,r} = -\frac{L_m}{L_s}\left(\frac{1}{\tau_s} + j\omega_r\right)\frac{V_s}{j\omega_s} e^{j\omega_s t_0} e^{-\frac{t}{\tau_s}} e^{j\omega_s(1-s)t} \qquad (9)$$

Where $\vec{v}_{rn}$ is the induced voltage in the rotor as a result of the DC (natural) flux component, and the superscript r represents the rotor reference frame. Disregard the term $\frac{1}{\tau_s}$, since it has a low value, the maximum amplitude of $\vec{v}_{rn}^{\,r}$, denoted by V_{rn}, happens at the moment of the voltage sag, represented as:

$$V_{rn}(t_0) = \frac{L_m}{L_s}(1-s)V_s \qquad (10)$$

Equation (10) illustrates the danger that may be encountered by the rotor circuit during grid voltage sags. Note that the pre-fault induced rotor voltage is proportional to the slip (s), while the induced rotor voltage during the voltage sag is proportional to $(1-s)$. Therefore, the induced voltage viewed from the rotor windings can be relatively large as a result of the grid fault since the rotor speed might be greater than the pre-fault slip speed. For example, consider that the DFIG is

This article has been accepted for publication in a future issue of this journal, but has not been fully edited. Content may change prior to final publication. Citation information: DOI 10.1109/TIA.2018.2835401, IEEE Transactions on Industry Applications

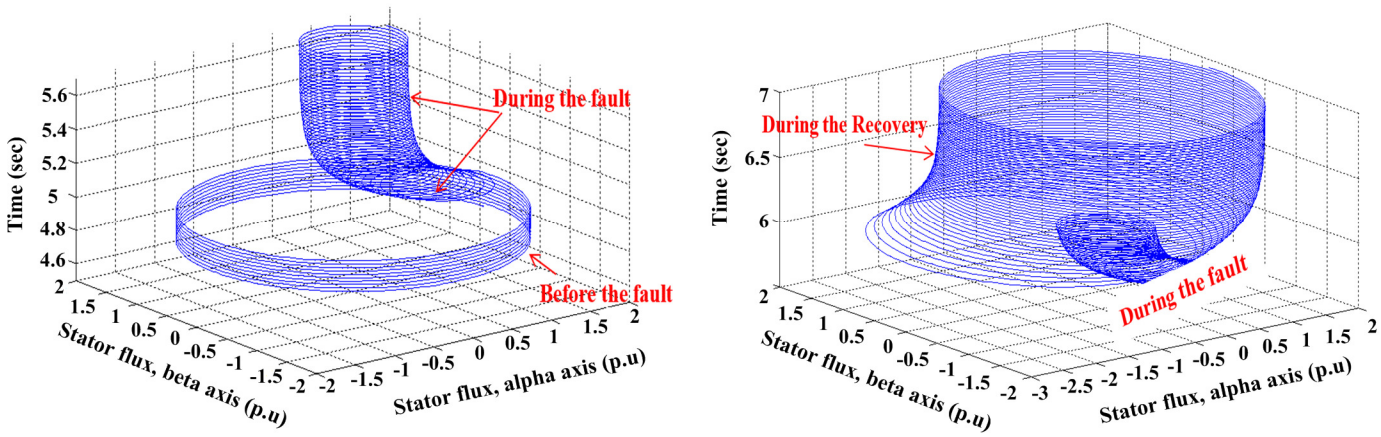

Fig. 8. 3-D plot of the $\alpha\beta$ stator flux linkage components before, during, after a three-phase step voltage sag.

initially running at the nominal speed, which is usually 30% above the synchronous speed (super-synchronous operating mode). This means that the pre-fault slip is $s = -0.3$. Assume that a three-phase-ground grid voltage sag happens at time t_0, which brings the stator terminal voltages down to zero. As a result, the rotor speed $\omega_r = (1 - s)\omega_s = 1.3\ \omega_s$. According to equation (10), the amplitude of the induced voltage, viewed from the rotor windings, increases 333% during the grid balanced fault. Moreover, the frequency of the induced voltage will also change. This results in an over voltage in the rotor circuit and will destroy the rotor power converter if not properly handled. If this happens, current components at two frequencies $s\omega_s$ and $\omega_r = (1 - s)\omega_s$ are produced. Since the rotor winding's resistance and leakage inductance are relatively small, the superposition of these two components will be large and the converter will not be able to control the rotor current. Furthermore, this scenario will force the converter to absorb a large amount of power, which causes problems of overvoltages in the DC bus [13], [28], [29].

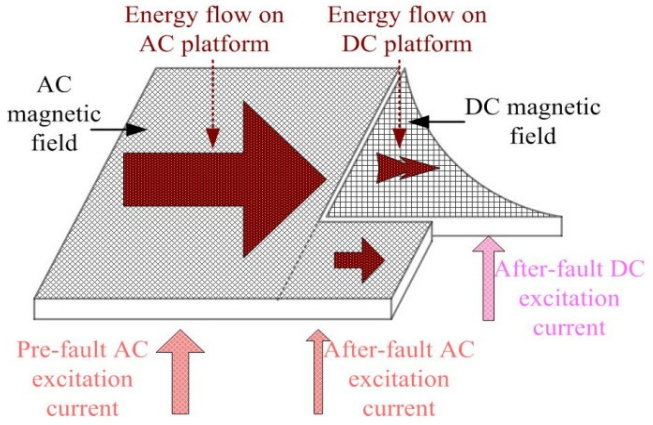

Fig. 9. Illustration of the energy flow before and after a three-phase voltage sag and its relationship to the stator flux linkage.

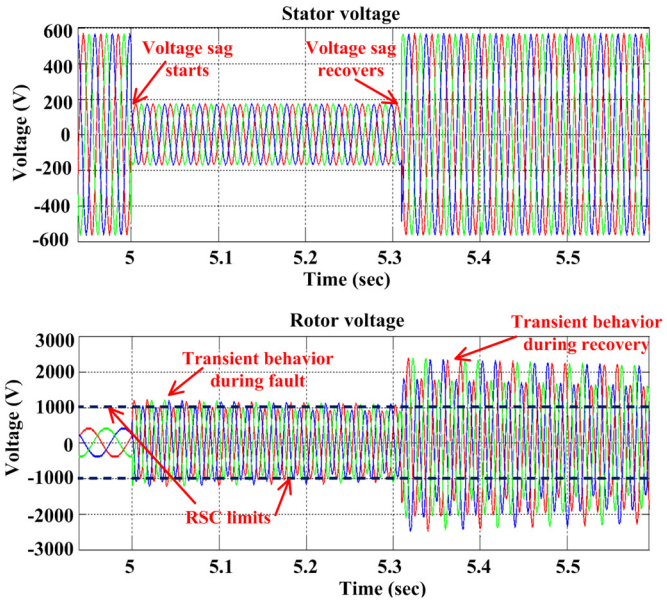

Fig. 10. Transient behavior of the three-phase rotor voltage during a three-phase grid voltage sag when the rotor current is tightly controlled to follow the command.

When analyzing recurring grid faults, analysis shows that the voltage recovery of the first grid fault will also introduce stator natural flux. If the stator natural flux is still present when the subsequent grid fault occurs, the stator natural flux produced by the voltage recovery and by the next voltage sag may be superposed [28]. Unless vector control is introduced before voltage recovery [30], [31], the stator natural flux will decay slowly after the voltage recovery of the first grid fault [32].

On average, the typical stator time constant of a large scale DFIG-based wind turbine is approximately 1 to 2 seconds. Furthermore, according to the grid code the shortest duration between two faults is only 500 milliseconds. This results in the transient currents and voltages being larger than those under a single fault [29]. This may cause the DFIG to fail to ride through the recurring faults even with the assistance of the rotor side crowbar. If the crowbar is triggered again during the recovery process, the rotor current can potentially accelerate the damping of the stator natural flux [29]-[31].

This article has been accepted for publication in a future issue of this journal, but has not been fully edited. Content may change prior to final publication. Citation information: DOI 10.1109/TIA.2018.2835401, IEEE Transactions on Industry Applications

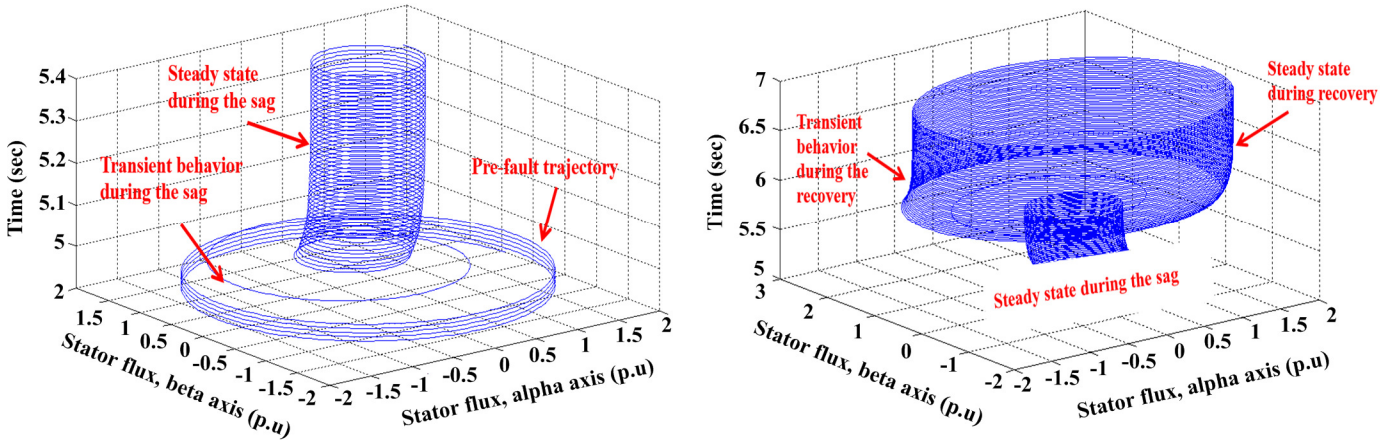

Fig. 11. 3-D plot of the $\alpha\beta$ stator flux linkage components before, during, and after a three-phase ramp voltage sag.

However, since at the time of recovery , the rotor current is not being controlled, the angle between the rotor current and the stator flux will fluctuate. This may introduce large electromagnetic torque fluctuations, which can compromise the reliability of the mechanical system. This introduces doubts as to whether the FRT strategies designed for single grid faults are the best solutions for the FRT of DFIG under recurring grid faults [13], [29].

Fig. 11 shows a 3-D plot of the simulated dq and $\alpha\beta$ stator flux linkage components during a three-phase partial voltage sag, respectively and stator flux trajectory of the DFIG during a balanced ramp voltage sag, respectively. The duration of the fault is 310 ms. The grid voltage sag happens at $t = 5\ sec$, and the PCC voltage drops to 30% of the normal operating condition within 30 ms. At $t = 5.310\ sec$, the grid fault is cleared by the protection system and system recovery begins.

The idea behind this test is to study the machine performance under the influence of a three-phase ramp voltage sag rather than having a step change. The simulation results prove that the effect of the grid voltage sag and recovery on the rotor circuit can be greatly reduced if they have a ramp nature instead of a sudden change. By comparing the 3-D stator flux trajectories during the three-phase step and ramp voltage sags, shown in Fig. 8 and Fig. 11, respectively, it is clear that the natural flux component is greatly reduced. The centers of the two trajectories (circles) during the fault and the recovery are the same without large transients. This is due to the fact that the ramp nature of the voltage sags helps to reduce the natural flux component that is generated during the fault in order to guarantee the continuity of the machine states.

Asymmetrical Faults

Asymmetrical faults are more common than three-phase faults in the power system. In this case, the stator flux may include positive and negative sequence components, as well as a transient DC component during grid faults [33]-[35].

Consider a single-phase to ground fault at the stator terminals of the DFIG at time $t = t_0$. This will bring the voltage of the faulted phase, e.g. phase a, to zero. Assuming that the positive and negative sequence networks have equal impedances, the voltages of the other two phases, i.e. b and c, will not change [24]. As a result, the stator flux during the voltage sag is expressed as [20], [22]:

$$\vec{\lambda}_s(t) = \underbrace{\frac{\vec{V}_1}{j\omega_s} e^{j\omega_s t}}_{\vec{\lambda}_{s1}} + \underbrace{\frac{\vec{V}_2}{-j\omega_s} e^{-j\omega_s t}}_{\vec{\lambda}_{s2}} + \underbrace{\vec{\lambda}_{sn0} e^{-\frac{t}{\tau_s}}}_{\vec{\lambda}_{sn}} \qquad (11)$$

where $\vec{\lambda}_{s1}, \vec{\lambda}_{s2}, \vec{\lambda}_{sn}$ are the positive, negative, and DC (natural) stator flux components. Fig. 12 shows the stator flux trajectory of a DFIG during a 50% single-phase-ground fault at the PCC starting at time $t = 0$. As stated earlier, in contrast to the three-phase balanced voltage sags, the initial value of the natural flux depends on the instant when the fault starts. In this case, since the fault starts at the moment when the positive and negative sequence flux components are aligned and their sum is equal to the pre-fault forced flux value, there is no natural (DC) flux. As a result, the stator flux of the DFIG will not have any transient behavior, as shown in Fig. 12.

Furthermore, the trajectory traced by the stator flux is elliptical during the asymmetrical voltage sags, as illustrated by Fig. 12. This is due to the fact that the positive sequence component produces a flux that rotates counterclockwise while the negative sequence component generates a flux that rotates clockwise. The major axis of the ellipse occurs when both fluxes coincide with the same direction while the minor axis appears when they are aligned but with opposite directions. Both situations happen twice per period [25]-[27], [32].

The worst case scenario happens when the voltage sag occurs at time $t = T/4$, where T is the grid period [20]. In this case, the natural flux reaches its maximum value since the positive and negative sequence components will generate fluxes that are completely in opposite direction and their sum is minimal [25], [26].

Fig. 13 shows the stator flux trajectory for a single-phase to ground fault that starts at $t_0 = T/4$. As shown, the natural flux causes the ellipse to have a DC offset from center. As a result, the stator flux trajectories before and after the fault are tangential. Furthermore, the natural flux reaches its maximum value, which maximizes the danger in the rotor circuit. As the natural flux component decays exponentially to zero with

This article has been accepted for publication in a future issue of this journal, but has not been fully edited. Content may change prior to final publication. Citation information: DOI 10.1109/TIA.2018.2835401, IEEE Transactions on Industry Applications

time, since it has a passive nature, the stator flux ellipse gradually moves to the center. It will be completely centered during steady-state conditions [23], [25], [26], [34].

Fig. 14 shows the simulated rotor voltage during a single-phase to ground grid voltage sag. The DFIG is operated in the super-synchronous speed mode with $s = -33\%$. In this test, the duration fault is 0.31 sec. The rotor current is tightly controlled to track the command. The analysis of the DFIG behavior is based on the decomposition of the stator flux into three components: the positive, the negative, and the natural fluxes. The positive flux, which rotates at synchronous speed, appears during the normal operation of the machine. It induces a voltage in the rotor proportional to the slip, which is relatively low. The negative flux appears due to the negative sequence component of the grid voltage. It rotates at synchronous speed in a reversed direction. The transient (natural) flux reaches its maximum value since the fault happens at $t_0 = T/4$ [25], [26], [34].

Fig. 15 illustrates the idea that the initial value of the natural flux, during asymmetrical faults, depends on the instant when the fault occurs. It also shows that, whether the current and magnetic flux DC components aggravate or mitigate the transients depends heavily on the phase (time) difference between the sag and recovery moments. As it can be seen, the transient behavior at the moment of recovery is minimized. This is due to the fact that the sag and recovery happen instantaneously and the time interval between the instances is of integer cycles. Therefore, the DC flux components counteract one another.

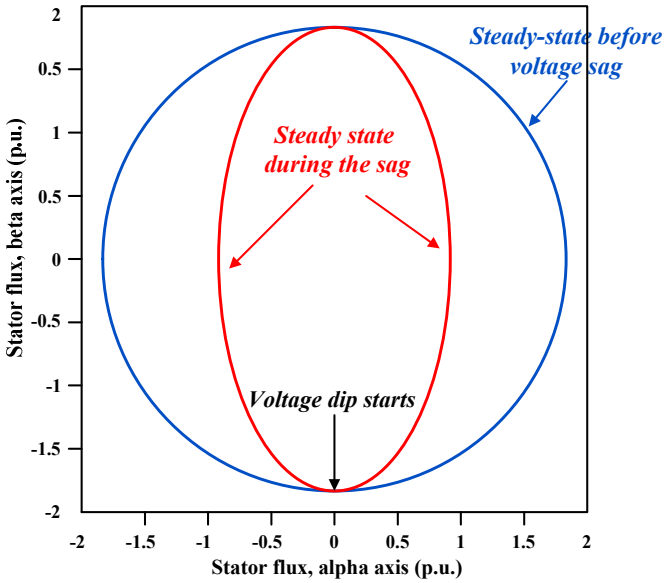

Fig. 12. Stator flux trajectory during a 50% single-phase to ground fault starting at time $t_0 = 0$.

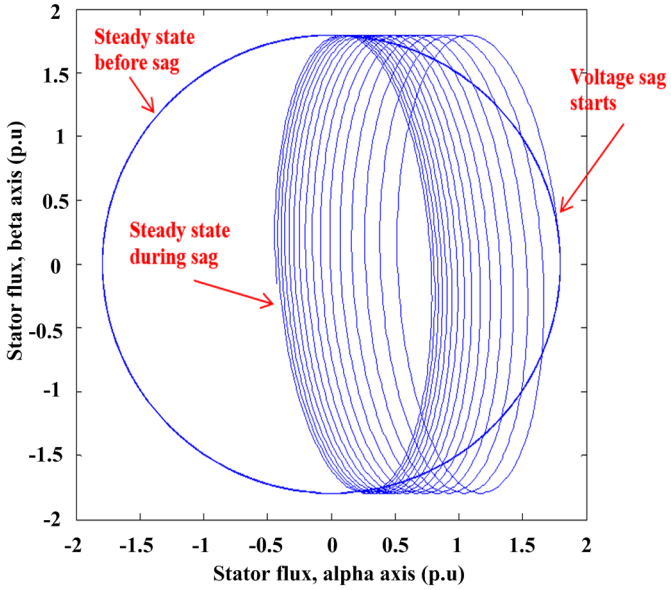

Fig. 13. Stator flux trajectory for a single-phase to ground fault beginning at $t_0 = T/4$.

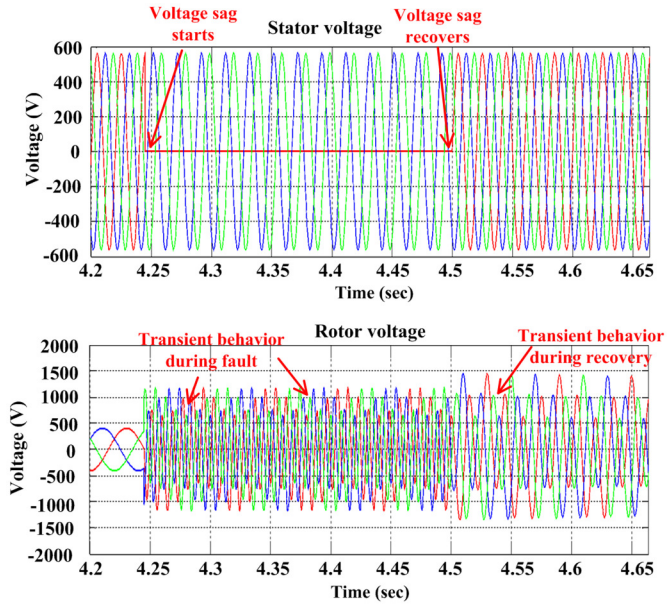

Fig. 14. Transient behavior of the three-phase rotor voltage during a single-phase to ground grid voltage sag when the rotor current is controlled tightly to follow the command.

This article has been accepted for publication in a future issue of this journal, but has not been fully edited. Content may change prior to final publication. Citation information: DOI 10.1109/TIA.2018.2835401, IEEE Transactions on Industry Applications

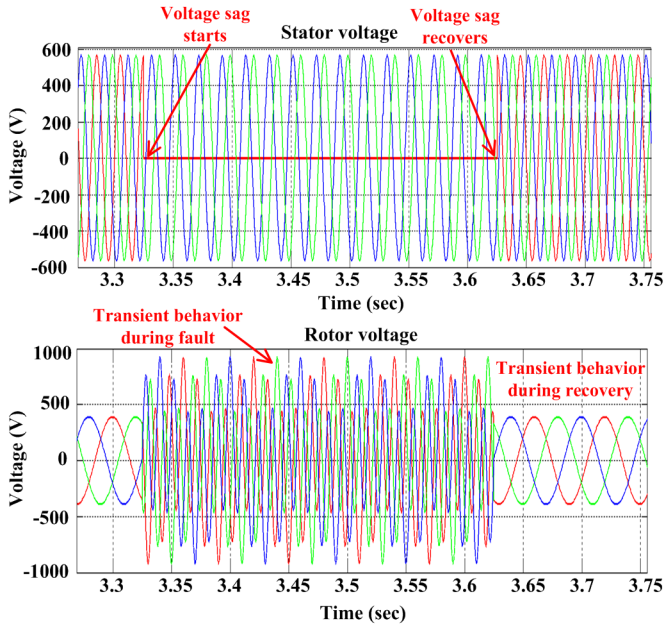

Fig. 15. Transient behavior of the three-phase rotor voltage during a single-phase to ground grid voltage sag. The DC flux components mitigate the transients during the recovery time since the phase difference between the moments of the sag and recovery is integer cycles.

III. LVRT of DFIG-Based Wind Turbines

A. Definition

The operation and grid connection requirements for wind turbines vary significantly from country to country and from power system to power system. These differences depend on the degree of wind power penetration and the robustness of the power network. Therefore, due to the relatively high level of wind power penetration, many European countries are currently leading the U.S. in developing new grid codes for wind turbines. A few of these requirements are summarized in [4], [6], [7].

LVRT or FRT capability during grid faults states that wind turbines are required to stay connected to the power grid for a specific amount of time before being allowed to disconnect. Moreover, wind turbines are required to exhibit a behavior similar to that of the conventional power plants and support the grid voltage during both symmetrical and asymmetrical grid voltage sags by means of reactive power compensation [4], [6].

A typical LVRT characteristic is shown in Fig. 16. According to the LVRT specification, wind turbines are required to stay connected to the grid and supply reactive power when the PCC voltage drops and falls in the blue area, as illustrated by Fig. 16. Furthermore, wind turbines must be able to operate continuously at V_f % of the rated PCC line voltage V_i, as seen in Fig. 16. The level of the voltage sag (V_x) and fault clearance time (T_x) are decided by the turbine protection system based on the location and type of fault, i.e. severity of the fault. The minimum value of V_x varies between countries and may equal zero depending on the LVRT characteristic adopted in each country. The slope of the recovery depends on the strength of the interconnection and reactive power support. Stronger systems can afford a much steeper increase and thus minimize the ride-through requirements of the generators [7], [10], [14], [16].

As previously mentioned, grid codes require that the wind turbines must have the capability to regulate reactive power within a certain range specified by the transmission system operator (TSO). They should also provide reactive power (up to 100% current capacity) to contribute to voltage recovery when grid voltage sag is present. This leads to larger MVA capacity during the design process of the whole converter system. As a result, satisfying this demand is relatively difficult to achieve via the DFIG-based wind turbine concept, shown in Fig. 2, with partially rated power converters. Other power quality units like STATCOMs may possibly be used to help the wind turbine system in achieving this hard requirement [17]. Fig. 17 shows the reactive current requirements for a wind farm during grid sags by German [35] and Danish grid codes [36].

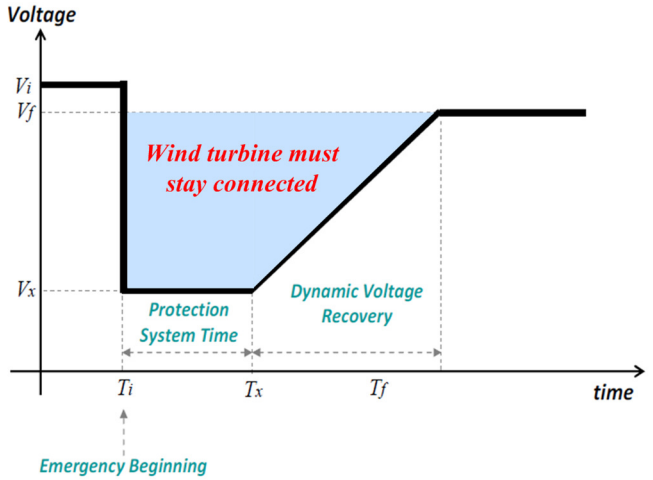

Fig. 16. Typical LVRT characteristic of a wind turbine or wind farm.

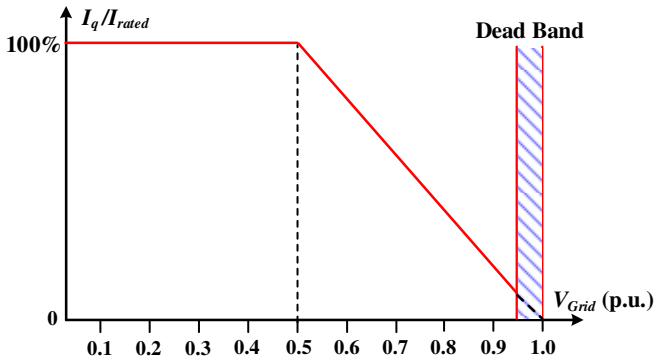

Fig. 17. Reactive current requirements for a wind farm during grid sags by German and Danish grid codes [35], [36].

B. LVRT Solutions

Section II showed that DFIG-based wind turbines are very sensitive to voltage dips during grid faults. This is due to the partial-scale back-back power converter. Faults in the power system, even those distant from the location of the turbine, can cause an abrupt drop in grid voltage that leads to an over-

This article has been accepted for publication in a future issue of this journal, but has not been fully edited. Content may change prior to final publication. Citation information: DOI 10.1109/TIA.2018.2835401, IEEE Transactions on Industry Applications

voltage in the DC bus and an over-current in the rotor circuit of the generator. Without any protection scheme, this will definitely lead to damage of the power converters. Moreover, it will also increase the speed of the turbine above the rated limits, which will threaten the safe operation of the turbine [34], [37]-[39]. Therefore, the LVRT ability of DFIG-based wind turbines under grid faults has been intensively studied in literature. Different solutions and strategies are being proposed and presented to achieve a reasonable LVRT of wind turbines. These LVRT strategies can be divided into two main groups:

1) LVRT solutions with hardware implementation (passive methods).
2) LVRT solutions by improving the RSC control strategies (active methods).

This subsection gives a detailed description of the most cited and commonly used LVRT solutions based on improving the RSC control strategies (active methods). It describes the operation principle, basic structure, advantages and disadvantages of each LVRT solution. LVRT solutions with hardware implementation are outside the scope of this paper.

LVRT solutions by improving the RSC control strategies (active methods).

Classical vector control, based on stator flux or stator voltage orientations, is normally used to achieve the independent control of active and reactive powers of DFIG using traditional PI controllers with either stator voltage orientation or stator flux orientation [40], [41]. This reduces the controller design complexity and achieves several control objectives.

The objective of the RSC controller is to obtain a decoupled control between the stator active and reactive powers injected into the grid. The control design consists of two cascaded loops; the inner current loop regulating the d- and q-axis rotor currents (i_{dr} and i_{qr}) and the outer control loop that regulates both active and reactive power, as shown in Fig. 18. The reference frame is selected such that it rotates synchronously with respect to the stator flux linkage (λ_s), with the d-axis aligned with the stator flux ($\lambda_{qs} = 0$), as shown in Fig. 19. This enables the RSC to control the electromagnetic torque and the stator reactive power independently. The direct axis current component (i_{dr}) is used to regulate the reactive power while the quadrature axis current (i_{qr}) is used to extract the desired electromagnetic torque (or stator output active power) [16], [24], [28], [40]. However, the d-q rotor currents are cross-coupled with the dq components of the RSC ac-side output voltages. Therefore, feedforward current regulators with PI controllers are commonly utilized to decouple the control of dq rotor currents [25], [28], [40]. The cross-coupling terms $\omega_{slip}\sigma L_r i_{qr}$ and $\omega_{slip}(L_{mm} i_{ms} + \sigma L_r i_{dr})$ are feedforward signals added to the outputs of the PI current controllers , as shown in Fig. 19, and compensate for the coupling effects. v_{dr}^* and v_{qr}^* are the reference values of the rotor voltages in d- and q-axis, respectively; i_{dr}^* and i_{qr}^* are the reference values of the rotor currents in d- and q-axis, respectively; P_s^* and Q_s^* are the reference values of the stator active and reactive power; respectively, ω_{slip} is the slip angular frequency; $\sigma = 1 - \frac{L_m^2}{L_s L_r}$; $L_{mm} = \frac{L_m^2}{L_s}$; i_{ms} is the magnetizing current; and all other symbols have the same meaning as previously defined in the paper.

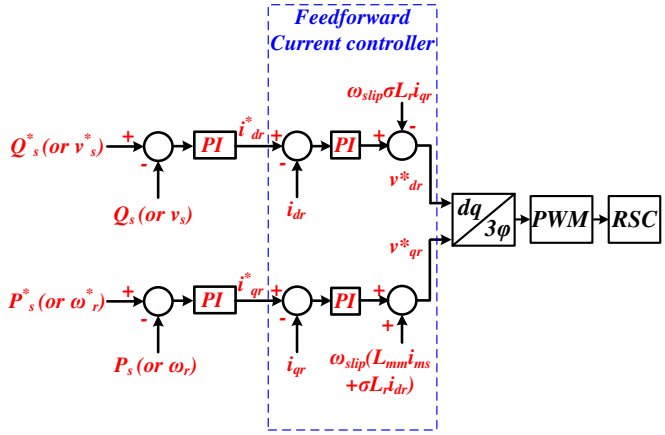

Fig. 18. Conventional vector control scheme for the RSC of DFIGs.

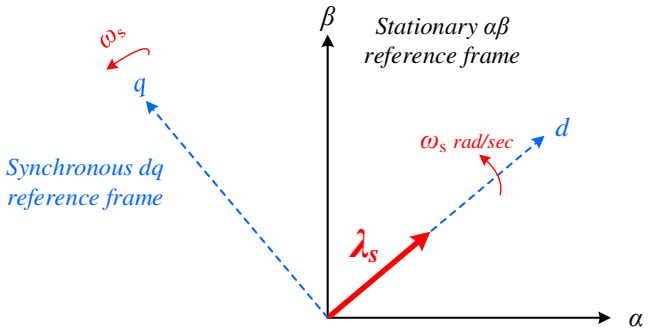

Fig. 19. The stator flux-oriented synchronous reference frame used for the RSC vector control scheme.

On the other hand, due to its limited bandwidth and gain margin, the effectiveness of PI controllers will be seriously degraded during grid voltage sags [41]-[43]. As a result, the independent control of DFIG is completely lost and it would be difficult to return to the effective regulated state. Furthermore, in addition to limiting the rotor current during the transient periods of stator voltage drop and recovery, it is important to limit the torque ripples that appear as a result of the stator voltage imbalance in order to reduce the gearbox stresses. Under asymmetrical grid faults and disturbances, second-order-harmonic ripples might appear in the electromagnetic torque, stator current, and stator active and reactive power outputs [42], [43].

It order to avoid all the aforementioned drawbacks of the classical vector control of DFIGs during grid faults and network imbalance conditions, much effort has been devoted to modify and improve the RSC control scheme in order to improve the dynamic operation of DFIG-based wind turbines and enhance their LVRT capability. This section will give an overview of the major control strategies proposed in literature to enhance the LVRT capability of DFIG-based wind turbines during grid faults (symmetrical and asymmetrical) and network harmonically distorted grid conditions.

This article has been accepted for publication in a future issue of this journal, but has not been fully edited. Content may change prior to final publication. Citation information: DOI 10.1109/TIA.2018.2835401, IEEE Transactions on Industry Applications

In [44], the authors showed that, during grid faults, DC and negative sequence components appear in the machine stator flux linkages, resulting in a large EMF induction in the rotor circuit. The proposed idea is based on eliminating undesired components in the stator-flux linkage by injecting the opposite components in the rotor current, with the intent to constrain the rotor current supplied to the RSC. The advantage of this method is that it can be applied to all types of symmetric and asymmetric grid faults. However, the proposed control strategy requires a fast observation of the stator flux linkage components. It also depends on the machine leakage inductance. Moreover, since the RSC is used to generate the rotor current, which is opposite to the transient component of the stator flux, the control effect is limited to the converter capacity.

In [45], the authors proposed an improved control scheme of the RSC that aims to reduce the current transients in the stator and rotor windings when a grid fault occurs. The idea is to feedback the measured stator currents as the set point for the current controller of the RSC when a voltage dip occurs. In this way, the current control system synthesizes rotor currents that generate current waveforms in the stator windings, with the same shape of the currents generated during the sag but in the counter phase. The control system under steady-state conditions would track the active and reactive power references. When a voltage sag at the stator terminals occurs, the external active and reactive power control loop gets disconnected, and the rotor currents set point will be changed to match the measured values of the stator currents in the dq reference frame. However, this strategy requires that the RSC voltage must be at least as high as the maximum rotor voltage during voltage dip to maintain current controllability. Otherwise, in the event of severe voltage dips, additional hardware protection is needed. This presents a limitation to the proposed strategy.

An improved DC-link voltage control strategy for DFIG-based wind turbines was proposed in [46]. It helps to reduce the magnitude of DC-link voltage fluctuations during grid faults. However, the proposed strategy does not examine the issues of rotor current transients during grid fault. Therefore, the proposed strategy does not have a major impact on improving the LVRT capability of DFIG-based wind turbines during grid faults.

In [47], the authors proposed two secondary voltage control schemes and a reactive power allocation strategy for a wind farm equipped with DFIG-based wind turbines. The allocation strategy includes the dispatch of reactive current to individual generators. It was shown that these strategies improve voltage regulation performance of the wind farm and also the voltage profile of the network in general. On the other hand, due to the small power ratings of the DFIG converters, the voltage control capability of the wind farm is limited. In a weak power network, the wind turbine generators may not be able to provide sufficient voltage control capability.

In order to improve the LVRT capacity of double-fed induction generator, non-linear controllers have also been used in the DFIG control system. A fuzzy controller, non-linear controller, reliable $H\infty$-based controller, exact linearization-based controller and predictive current controller were proposed in [48]-[52], respectively. However, these control schemes are very complicated in a practical application, as they require a quantity of calculations that are not possible in real-time applications. Moreover, in a weak power network, there is a risk of voltage instability that may result in the tripping of wind turbine generators.

In practice, unbalanced grid voltage is common in weak grid areas and offshore sites. Furthermore, with the development of grid-connected devices and energy systems, there will be a wide variety of non-linear loads and power electronic devices connected to the grid directly in the near future. All these ongoing changes have a great impact on the stability of the conventionally controlled DFIG system due to the presence of unbalanced grid voltage [48, 53].

Direct power control (DPC) approaches were proposed in [53]-[56] to minimize the second-order-harmonic torque ripples that appear during grid faults. Following these approaches, the positive- and negative-sequence components of the DFIG stator active and reactive power outputs are first separated. Then, combinations of these power components can be controlled directly by DPC to accomplish the following three conditions: 1) eliminating the torque and stator reactive power ripples, 2) eliminating the stator current ripples, and 3) eliminating the stator active and reactive power ripples [56].

In [57], the authors proposed an enhanced control scheme to improve the dynamic behavior of the DFIG-based wind turbine under distorted grid voltage conditions. A proportional integral plus resonant (PI-R) current controller in the synchronously rotating (dq) reference frame is employed to simultaneously regulate the fundamental and harmonic components of rotor currents without any sequential component decomposition.

In [58] and [59], the authors proposed a combined positive and negative sequences control (CPNSC) scheme for grid-connected voltage source converters under an unbalanced grid voltage condition. It was shown that the second harmonic can be reduced by either filters or a Delayed Signal Cancellation (DSC) approach.

In [60], a DFIG positive sequence control scheme was proposed to improve the DFIG performance under polluted grid conditions. The controller is designed using a bandpass filter feeding into a standard lead-lag controller. It was utilized to remove the second harmonic from the torque by generating the rotor compensating voltage from the observed torque pulsation.

In [61], a feed-forward transient current control scheme was proposed to improve the LVRT capability of the DFIG during three-phase grid faults. The new control strategy targets the RSC of the DFIG. It introduces additional feed-forward transient compensations to the conventional current regulator of the RSC. The purpose is to provide a mechanism that can correctly align the RSC AC-side output voltage with the transient induced voltage. The authors proved that the proposed control scheme is able to minimize the transient rotor current and the occurrence of crowbar interruptions.

This article has been accepted for publication in a future issue of this journal, but has not been fully edited. Content may change prior to final publication. Citation information: DOI 10.1109/TIA.2018.2835401, IEEE Transactions on Industry Applications

IV. Proposed Rotor-Side Control Scheme For DFIG-Based Wind Turbines To Ride-Through Symmetrical Grid Faults

Based on the theoretical exploration of the complicated dynamic behavior of the DFIG-based wind turbine during grid faults presented in Section II, this part of the paper presents a new rotor-side control scheme for the DFIG to enhance its LVRT capability during severe symmetrical grid voltage sags. The proposed control strategy mitigates the rotor-side voltage and current shock during grid abnormal conditions, without any additional cost or reliability issues. As a result, the DFIG performance is improved and utility company standards are fulfilled.

Discussion starts with developing a mathematical model for the stator natural flux (DC) component that appears during grid voltage dips. Then, the proposed control strategy is described and implemented. Finally, computer simulations are used to verify the expanded ride-through capability of the novel strategy and its effective performance compared to the conventional control schemes

A. Mathematical Model of the Natural (DC) Flux Component during Symmetrical Voltage Sags

As mentioned in Section II, the DC magnetic field in the air gap is the major concern in LVRT control. In the following analysis, a three-phase-ground symmetrical fault is assumed at PCC. Then, a DC field component is generated, possibly triggering the collapse of the system. The DC component can be split in two components and the following equations are produced [62]:

$$\begin{cases} 0 = r_s i_{ds\_dc} + \dfrac{d\lambda_{ds\_dc}}{dt} \\ 0 = r_s i_{qs\_dc} + \dfrac{d\lambda_{qs\_dc}}{dt} \\ v_{dr\_dc} = r_r i_{dr\_dc} + \dfrac{d\lambda_{dr\_dc}}{dt} + (\omega_r)\lambda_{qr\_dc} \\ v_{qr\_dc} = r_r i_{qr\_dc} + \dfrac{d\lambda_{qr\_dc}}{dt} - (\omega_r)\lambda_{dr\_dc} \\ \lambda_{ds\_dc} = L_s i_{ds\_dc} + L_m i_{dr\_dc} \\ \lambda_{qs\_dc} = L_r i_{qs\_dc} + L_m i_{qr\_dc} \\ \lambda_{dr\_dc} = L_r i_{dr\_dc} + L_m i_{ds\_dc} \\ \lambda_{qr\_dc} = L_r i_{qr\_dc} + L_m i_{qs\_dc} \end{cases} \quad (12)$$

where all variables and subscripts share the same meaning as those defined in the system of equations (1), but are designated to the DC components. If the d-axis of the DC transient components is also oriented toward the stator DC-Flux direction, the q-axis component λ_{qs_dc} becomes zero, and the above equations can be simplified to:

$$\frac{d\lambda_{ds\_dc}}{dt} = -R_s i_{ds\_dc} \quad (13)$$

$$\lambda_{ds\_dc} = L_s i_{ds\_dc} + L_m i_{dr\_dc} \quad (14)$$

$$0 = L_s i_{qs\_dc} + L_m i_{qr\_dc} \quad (15)$$

$$i_{qs\_dc} = -\frac{L_m}{L_s} i_{qr\_dc} \quad (16)$$

$$i_{dr\_dc} = \frac{\lambda_{ds\_dc}}{L_m} - \frac{L_s}{L_m} i_{ds\_dc} \quad (17)$$

Equations (13)-(17) show that the transient DC current components could be on both the stator and rotor. The splitting of the current on the stator and the rotor is determined by the pre-fault instant. Equation (15) can be transformed to (16), indicating the proportional relationship between the q-axis DC current (torque current) on the stator and rotor. Furthermore, equation (13) shows that the decay of DC flux is determined by the stator circuit resistance and its DC current. Fig. 20 shows the extracted stator flux DC component, from Fig. 5, during a three-phase-ground grid voltage sag. It can be seen that the fault at the stator terminal triggers the flux fluctuation. Since the machine states must be continuous, a natural (DC) component appears in the stator flux to compensate for the difference in stator flux and guarantee its continuity.

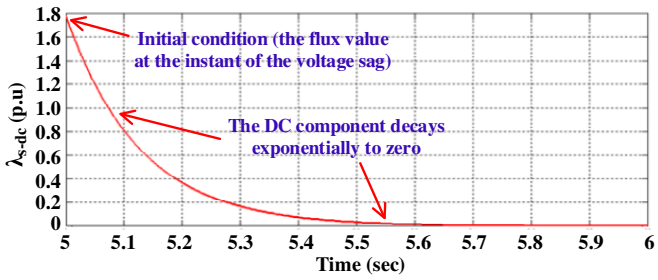

Fig. 20. The extracted stator flux DC component, from Fig. 5, during a symmetrical grid voltage sag.

B. Proposed Control Strategy during Symmetrical Grid Voltage Sags

As mentioned, the DC magnetic field in the air gap is the major concern in LVRT control. Equation (13) shows that the DC flux linkage can be adjusted by changing either the stator resistance or the DC component of the stator winding current. Equation (13) can be rewritten as equation (18) if the transmission line stray resistance is taken into account.

$$\frac{d\lambda_{ds\_dc}}{dt} = -(R_s + R_{stray}) i_{ds\_dc} \quad (18)$$

The main objective of the control strategy is to accelerate the decay of the DC component of the stator flux linkage. Equation (18) shows that the changing rate of the stator DC flux linkage is associated with the stator resistance R_s, transmission line stray resistance R_{stray} and the DC component of the stator winding current i_{ds_dc}. Therefore, there are two ways to control the stator DC flux linkage:

1) Changing the resistance of the stator winding.
2) Applying active control to the DC component of the stator winding current.

Changing resistance of the stator winding is a less favored approach because the resistors used for current decay must handle high energy and power and are therefore bulky. Moreover, cut-in and cut-off of the resistors will introduce additional transient into the system. The main objective of the

This article has been accepted for publication in a future issue of this journal, but has not been fully edited. Content may change prior to final publication. Citation information: DOI 10.1109/TIA.2018.2835401, IEEE Transactions on Industry Applications

proposed control method is to find a way to accelerate the decay of the stator DC Component as quickly as possible, indirectly controlled by the rotor side converter, without inserting additional stator resistance.

Disregarding stator and rotor leakage inductance, the corresponding induced rotor voltage vector leads the stator DC flux linkage by 90 degrees. Normally, the RSC is designed to control the rotor current in slip frequency. Therefore, for the stator DC flux induced voltage in rotor frequency, the RSC acts like variable impedance. Since the PI current controllers, as well as the DC link voltage, are not strong enough to reject all currents and voltages in other frequencies, the stator DC flux induced current i_{r_dc} in the rotor frequency appears in the rotor circuit, which lags to v_{r_dc} by certain degrees (the rotor circuit and RSC is inductive), as shown in Fig. 21(a). λ_{s_dc} is the transient stator DC flux linkage and i_{s_dc} is its excitation current.

This rotor current will affect the magnetic field and introduce another DC current component $i_{sdc\_balance}$ on the stator to balance the magnetic field from sudden variation. The original stator DC flux excitation current, i_{s_dc}, together with this balance current, $i_{sdc\_balance}$, is combined to form the final stator DC current, $i_{sdc\_synthesis}$, that can help damp out the passive DC flux.

The current in the above description gives a natural decay of the stator DC flux component without any active control by the RSC. The control strategy we apply here is to optimize the DC stator flux change trajectory.

In the proposed control strategy, we consider the normal current control in slip frequency and the active current control in rotor speed frequency for forced decay of stator DC flux together. Fig. 21(b) illustrates the controlled current vector diagram for forced decay of stator DC flux. According to equation (18), to accelerate and eliminate the stator DC flux component means to maximize the stator DC current. Here we attempt to maximize the DC damping effect by aligning the rotor current in rotor frequency to the opposite direction of the stator DC flux. In this manner, the rotor current will increase the stator current vector from i_{s_dc} to $i_{sdc\_synthesis}$, and speed up the DC flux decay for the stator [62].

The aforementioned proposed control strategy is embedded into the RSC control system. Fig. 22 shows the schematic of the overall RSC control system, including the proposed LVRT control scheme. $i^*_{dr\_dc}$ and $i^*_{qr\_dc}$ are the reference values of the DC flux linkage damping currents in *d*- and *q*-axis, respectively; λ_{s_dc} is the transient stator DC flux linkage; λ_{dqs_P} and λ_{dqs_N} are the positive and negative sequence components of the stator linkage in *d*- and *q*-axis, respectively; all other symbols have the same meaning as previously defined in the paper. In addition to the conventional vector control blocks, a stationary stator flux calculation and detection unit has been added to the RSC control scheme to primarily detect λ_{s_dc}, as shown in Fig. 23.

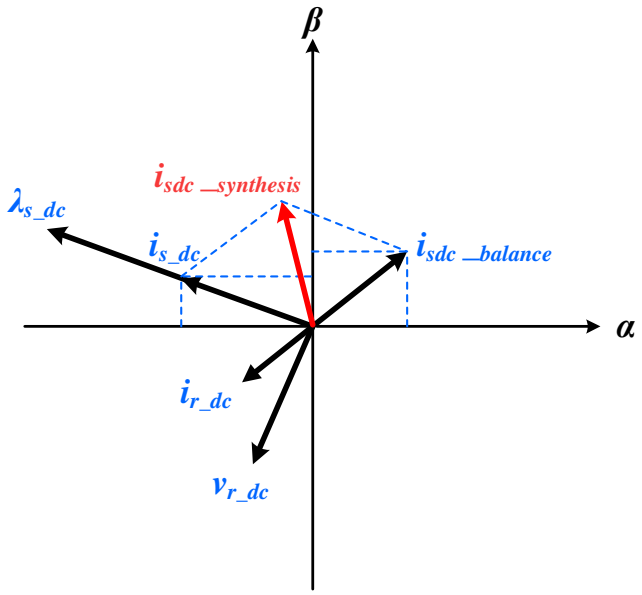

(a) Without extra rotor current control.

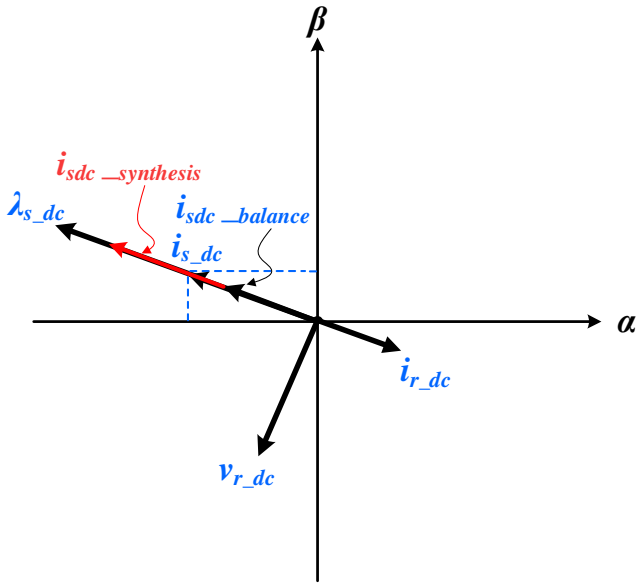

(b) With proposed rotor current control.

Fig. 21. DC components vector relationship.

C. Simulation Results and Analysis of the Proposed Control Strategy

MATLAB/Simulink-based simulations have been carried out to verify the proposed low voltage ride through control strategy. The specifications and relevant parameters of the DFIG system are listed in Table.1.

Two cases were simulated and the results were compared to each other to verify the effectiveness of the proposed algorithm. For all cases, a grid fault occurs at 7.9 sec and the grid side voltage drops to 30% of the normal operating condition. At 8.21 sec, the grid fault is removed and the system recovery begins.

Case 1: Unlimited DC bus voltage is assumed and the rotor current is controlled tightly to track the command using the conventional vector control scheme.

Case 2: The rated DC bus voltage is assumed and the proposed transient current control is applied.

Since unlimited DC bus voltage is assumed, the results in Case 1 are satisfactory in rotor side current, as shown in Fig. 24. However, the rotor voltage is excessively high during the grid voltage sag and recovery, and exceeds the RSC output voltage limit. Fig. 25 shows the simulation results of the three-phase rotor voltage and current when the proposed novel RSC control scheme is applied. The results clearly show that both the RSC voltage and rotor current are controlled satisfactorily within the achievable range and low voltage ride through is fulfilled.

The proposed and conventional control strategies are also compared in terms of DC bus voltage and rotor electromagnetic torque. Fig. 26 shows those waveforms with a conventional control strategy and Fig. 27 shows the novel proposed control strategy. In Fig. 26, the DC bus is overcharged during fault and is far beyond the maximum voltage limit. The torque waveform with oscillation superimposed has a constant offset, as shown in Fig. 26. Torque offset is generated by the DC magnetic field and the oscillation is due to AC and DC magnetic field interaction. With the novel control strategy, shown in Fig. 27, the DC bus voltage and torque waveforms are regulated within limits. The DC bus voltage oscillation is less than 100 volts, which falls within the safe operation area. The torque waveform doesn't have offset and its oscillation is damped out gradually. As discussed previously in Fig. 21(a) and Fig. 21(b), the one with conventional control has active power flow from the turbine to the rotor side on DC magnetic field, which serves to explain the torque offset in Fig. 26. However, with the proposed control method, the rotor DC voltage and current are perpendicular to one another, which does not introduce any active power to the rotor side [62].

V. CONCLUSION

This paper presents a detailed investigation of the LVRT of grid-connected DFIGs. It provides a detailed investigation of the dynamic behavior of DFIG-based wind turbines during different types of grid voltage sags. The analysis shows that the main reason behind the dynamic response of the DFIG to a grid voltage transient is the DC (natural) stator flux linkage component, which is a transient component that is fixed to the stator. It appears as the magnetic field is continuous and there is no discontinuity in the state variables of the generator. The DC stator flux linkage component induces high oscillatory rotor voltages in the rotor circuit. Depending on the severity of the sag, the voltage induced by natural flux can be much higher than the rotor rated voltage. Therefore, this will result in the saturation of the rotor converter.

In regards to the recurring grid faults, the analysis shows that the voltage recovery of the first grid fault also introduces the stator natural flux. If this stator natural flux still exists when the subsequent grid fault occurs, the stator natural flux produced by the voltage recovery and by the next voltage sag may be superposed. This may cause the DFIG to fail to ride through the recurring faults, even with the assistance of the rotor side crowbar. As a result, the FRT strategies designed for single grid faults do not provide the best solution for the FRT of the DFIGs under recurring grid faults.

This paper also presents a detailed description of the most cited and commonly used LVRT solutions for DFIG-based wind turbines by improving the RSC control strategies (active methods). It describes the basic operation principle, as well as advantages and disadvantages of each proposed solution. Finally, a new rotor-side control scheme to enhance the LVRT capability of DFIGs-based wind turbines during severe grid voltage sags is proposed. The control strategy is directed at mitigating the rotor-side voltage and current shock during abnormal grid conditions, without any additional cost or reliability issues.

This article has been accepted for publication in a future issue of this journal, but has not been fully edited. Content may change prior to final publication. Citation information: DOI 10.1109/TIA.2018.2835401, IEEE Transactions on Industry Applications

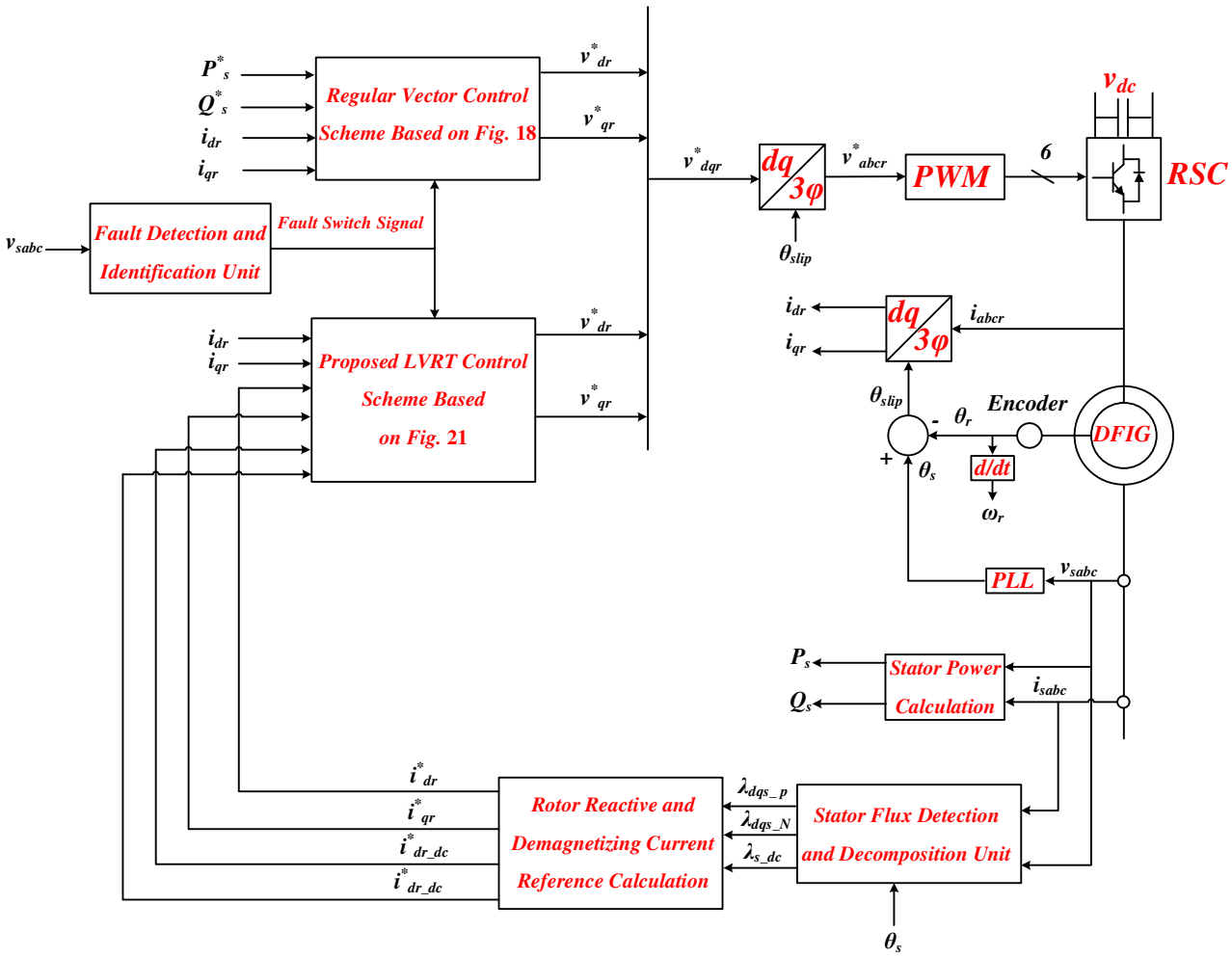

Fig. 22. Schematic of the overall RSC control system, including the proposed LVRT control scheme.

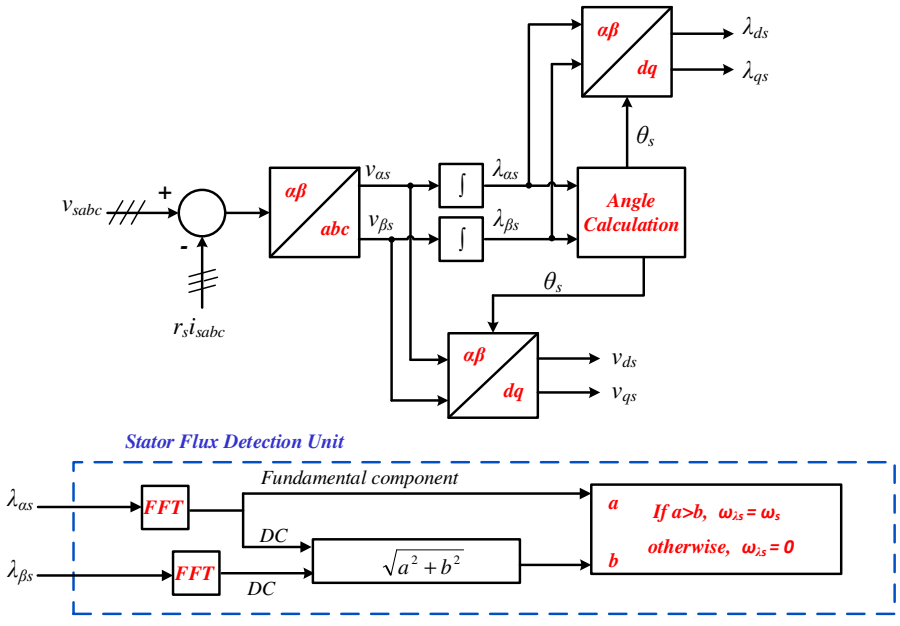

Fig. 23. Stationary stator flux calculation and detection units.

This article has been accepted for publication in a future issue of this journal, but has not been fully edited. Content may change prior to final publication. Citation information: DOI 10.1109/TIA.2018.2835401, IEEE Transactions on Industry Applications

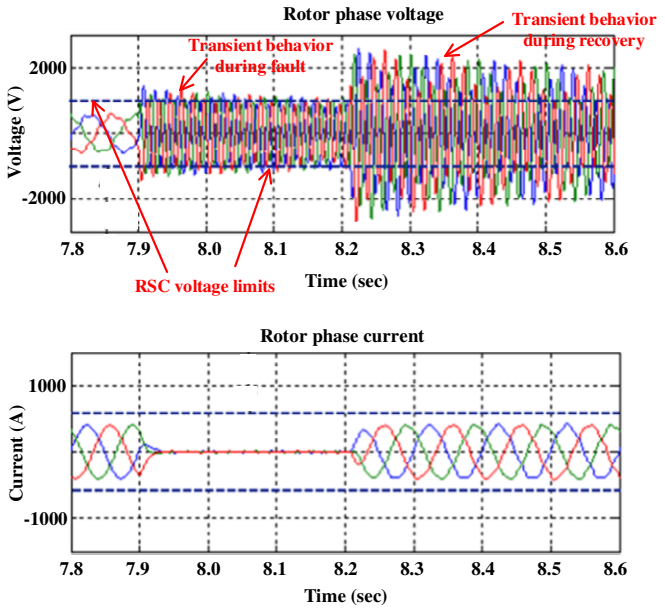

Fig. 24. Transient behavior of the three-phase rotor voltage and current during a three-phase grid voltage dip when the rotor current is controlled tightly to follow the command and unlimited DC bus is assumed.

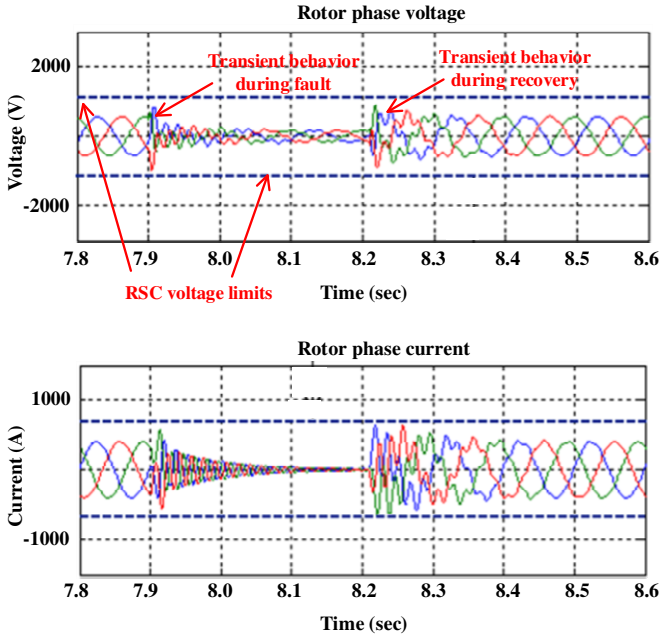

Fig. 25. Transient behavior of the three-phase rotor voltage and current during a three-phase grid voltage dip using the proposed control algorithm.

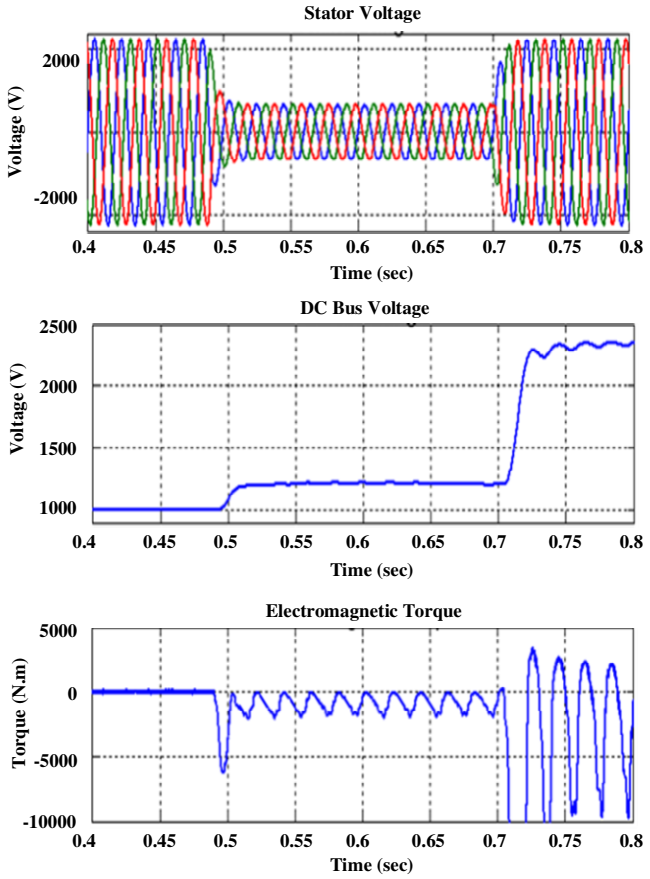

Fig. 26. DFIG DC bus voltage and torque during fault with the conventional vector control strategy.

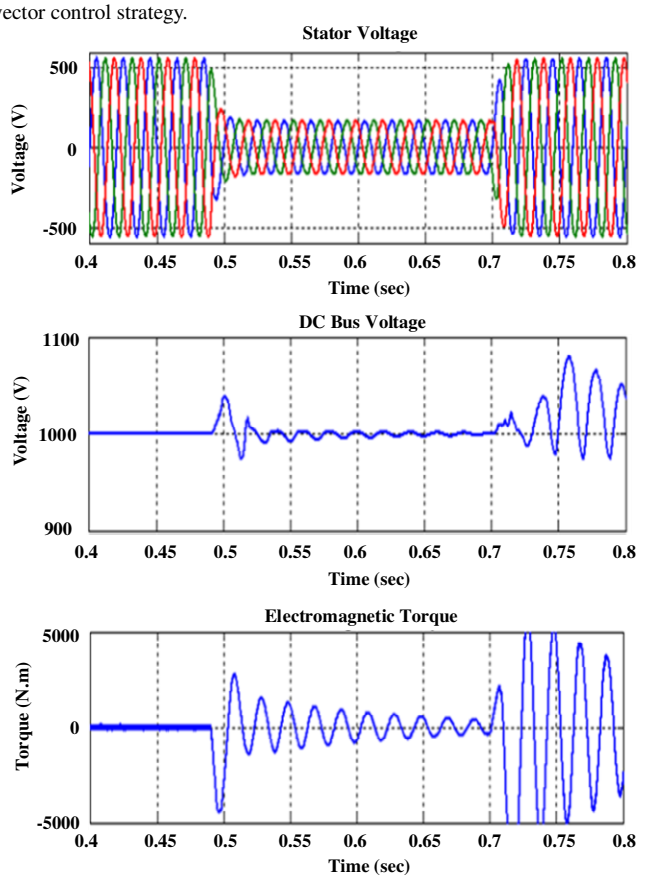

Fig. 27. DFIG DC bus voltage and torque during fault with the proposed control strategy.

ACKNOWLEDGMENT

The authors are grateful for the partial financial support provided by State Key Laboratory of Alternate Electrical Power System with Renewable Energy Sources, North China Electric Power University, China.

REFERENCES

[1] Y. Alsmadi, L. Xu, F. Blaabjerg, A. Pina Ortega, and A. Wang, "Comprehensive Analysis of the Dynamic Behavior of Grid-Connected DFIG-Based Wind Turbines under LVRT Conditions," In *Proc. 2015 IEEE Energy Conversion Congress & Exposition (ECCE 2015)*, Montreal, Canada, 2015, pp. 4178 - 4187.

[2] "Renewables 2016 global status report," Renewable Energy Policy Network for the 21st Century (REN21), November 2016 (available online at: http://www.ren21.net/category/ren21-Publications).

[3] "20% wind energy by 2030: increasing wind energy's contribution to U.S. electricity supply," U.S. Department of Energy, May 2008 (available online at: http://www.eere.energy.gov/windandhydro).

[4] W. Qiao and R.G. Harley, "Grid connection requirements and solutions for DFIG wind turbines," In *Proc. IEEE Energy 2030 Conference*, Atlanta, GA, 2008, pp. 1-8.

[5] V. Akhmatov, "Analysis of dynamic behavior of electric power systems with large amount of wind power," Ph.D. thesis, Technical University of Denmark, Kgs. Lyngby, Denmark, 2003.

[6] FERC - Interconnection of Wind Energy, 18 CFR Part 35, Docket No. RM05-4-001; Order No. 661-A December 12, 2005.

[7] C. Abbey and G. Joos, "Effect of low voltage ride through (LVRT) characteristic on voltage stability," in *Proc. IEEE PES General Meeting*, San Francisco, CA, USA, June 12-16, 2005, pp. 1901-1907.

[8] A. Hansen, P. Sorensen, F. Iov, and F. Blaabjerg, "Review of contemporary wind turbine concepts and their market penetration," *Wind & Solar Energy journal*, vol. 28, issue 3, 2004.

[9] H. Li and Z. Chen, "Overview of different wind generator systems and their comparisons," *IET Renewable Power Generation*, vol. 2, no. 2, pp. 123-138, August 2007.

[10] J. Morren and S.W.H. de Haan, "Ridethrough of wind turbines with doubly-fed induction generator during a voltage dip," *IEEE Trans. Energy Convers.*, vol. 20, no. 2, pp. 435 – 441, June 2005.

[11] J. Lopez, P. Sanchis, X. Roboam, and L. Marroyo, "Dynamic behavior of the doubly fed induction generator during three-phase voltage dips," *IEEE Trans. Energy Convers.*, vol. 22, no. 3, pp. 709 – 717, Sept. 2007.

[12] X. Kong, Z. Zhang, X. Yin and M. Wen, "Study of fault current characteristics of the DFIG considering dynamic response of the RSC," *IEEE Trans. Energy Convers.*, vol. 29, no. 2, pp. 278-287, June. 2014.

[13] W. Chen, F. Blaabjerg, N. Zhu, M. Chen and D. Xu, "Doubly fed induction generator wind turbine system subject to symmetrical recurring grid faults", *IEEE Trans. Power Electron.,* early access, 2015.

[14] S. Seman, J. Niiranen, S. Kanerva, A. Arkkio, and J. Saitz, "Performance study of a doubly fed wind-power induction generator under network disturbances," *IEEE Trans. Energy Convers.*, vol. 21, no. 4, pp. 883 – 890, December 2006.

[15] I. Erlich, H. Wrede, and C. Feltes, "Dynamic behavior of DFIG-based wind turbines during grid faults," in *Proc. 38th IEEE Power Electronics Specialists Conference,* Orlando, FL, USA, June 17-21, 2007, pp. 1195-1200.

[16] A. Hansen, G. Michalke, P. Sørensen, F. Iov, and T. Lund, "Co-ordinated voltage control of DFIG wind turbines in uninterrupted operation during grid faults," *Wind & Solar Energy Journal*, vol. 10, no. 1, Aug. 2006.

[17] F. Blaabjerg and K. Ma, "Future on power electronics for wind turbine systems," *IEEE Journal of Emerging and Selected Topics in Power Electron.*, vol. 1, no. 3, pp. 139-152, Sept. 2013.

[18] H. Li and Z. Chen, "Overview of different wind generator systems and their comparisons," *IET Renewable Power Generation*, vol. no.2, issue 2, pp. 123-138, August 2007.

[19] F. Blaabjerg, M. Liserre, and K. Ma, "Power Electronics Converters for Wind Turbine Systems," *IEEE Trans. Ind. Appl.*,vol. 48, no. 2, pp. 708-719, 2012.

[20] A. D. Hansen, P. Sorensen, F. Iov, and F. Blaabjerg, "Control of variable speed wind turbines with doubly-fed induction generators," *Wind Engineering*, vol. 28, no. 4, pp. 411–434, 2004.

[21] Y. Lei, A. Mullane, G. Lightbody, and R. Yacamini, "Modeling of the wind turbine with a doubly fed induction generator for grid integration studies," *IEEE Trans. Energy Conversion*, vol. 21, no. 1, March, 2006, pp. 257-264.

[22] D. W. Novotny and T. A. Lipo, "Vector control and dynamics of AC drives," Oxford University Press, 2000. ISBN-13: 978-0198564393.

[23] F. K. A. Lima, A. Luna, P. Rodriguez, E. H. Watanable and F. Blaabjerg, "Simplified modeling of a DFIG for transient studies in wind power applications," *IEEE Trans. Ind. Electron.,* vol. 58, no. 1, Jan 2011.

[24] J. Liang, W. Qiao, and R. G. Harley, "Feed-forward transient current control for low-voltage ride-through enhancement of DFIG wind turbines," *IEEE Trans. Energy Convers.*, vol. 25, no. 3, pp. 836-843, Sept. 2010.

[25] F. Lima, A. Luna, P. Rodriguez, E. Watanable, and F. Blaabjerg, "Rotor voltage dynamics in the doubly-fed induction generator during grid faults," *IEEE Trans. Power Electron.*, vol. 25, no. 1, pp. 118-130, 2010.

[26] J. Lopez, E. Gubia, P, Sanchis, X. Roboam, and L. Marroyo, "Wind turbines based on doubly fed induction generator under asymmetrical voltage dips," *IEEE Trans. Energy Convers.*, vol. 23, no. 4, pp. 321–330, 2008.

[27] V. F. Mendes, C. V. Sousa, S. R. Silva, B. Rabelo, S. Krauss and W. Hofmann, "Modeling and ride-through control of doubly fed induction generators during symmetrical voltage sags," *IEEE Trans. Energy Convers.*, vol. 26, no. 4, pp. 1161 – 1171, 2011.

[28] D. Xiang, L. Ran, P. J. Tavner and S. Yang, "Control of a doubly-fed induction generator in a wind turbine during grid fault ride-through," *IEEE Trans. Energy Convers.*, vol. 21, no. 3, pp. 652- 662, 2006.

[29] W. Chen, D. Xu, N. Zhu, M. Chen, and F. Blaabjerg, "Control of doubly fed induction generator to ride through recurring grid faults," *IEEE Trans. Power Electron*, early access, 2015.

[30] G. Pannell, D.J. Atkinson, B. Zahawi, "Minimum-threshold crowbar for a Fault-Ride-Through grid-code-compliant DFIG wind turbine," *IEEE Trans. Energy Convers.*, vol. 25, no. 3, pp. 750-759, 2010.

[31] J. Vidal, G. Abad, J. Arza and S. Aurtenechea, "Single-phase DC crowbar topologies for low voltage ride through fulfillment of high-power doubly fed induction generator-based wind turbines", *IEEE Trans. on Energy Convers.*, vol. 28, no.3, pp. 435-441, 2013.

[32] M. Mohseni, S.M. Islam and M.A.S. Masoum, "Impacts of symmetrical and asymmetrical voltage sags on DFIG-based wind turbines considering phase-angle jump, voltage recovery, and sag parameters", *IEEE Trans. Power Electron.*, vol. 26, no.5, pp. 1587-1598, May 2011.

[33] M. Bollen, G. Olguin, M. Martins, "Voltage dips at the terminals of wind power installations," *Wind Energy*, vol. 8, no. 3, pp. 307-318, 2005.

[34] S. Xiao, G. Yang, H. Zhou and H. Geng, "Analysis of the control limit for rotor-side converter for doubly fed induction generator-based wind energy conversion system under various voltage dips", *IET Ren. Power Gen.*, vol.7, iss. 1, pp. 71-81, 2013.

[35] *Technical Regulation 3.2.5 for Wind Power Plants with a Power Output Greater than 11 kW*, Energinet, Fredericia, Denmark, Sep. 2010.

[36] *Requirements for Offshore Grid Connections in the E.ON Netz Network*, E.ON-Netz, Bayreuth, Germany, Apr. 2008.

[37] J. Yao, H. Li, Z. Chen, X. Xia, X. Chen, Q. Li, Y. Liao, "Enhanced control of a DFIG-based wind-power generation system with series grid-side converter under unbalanced grid voltage conditions," *IEEE Trans. Power Electron.* , vol. 28, no.7, pp. 3167-3181, Jul. 2013.

[38] B.I. Naess, J. Eek, T.M. Undeland, and T. Gjengedal, "Ride through solutions for doubly fed induction generators," In *Proc. World Wind Energy Conference and Renewable Energy Exhibition*, Melbourene, Australia, Novemebr, 2005.

[39] C. Abby, W. Li, G. Goos, L. Owatta, "Power electronics converter control techniques for improvement low voltage ride through performance in wind turbine generators," in *Proc. Power Electronics Specialists Conference (PESC)*, June, 2006, pp. 1-6.

[40] R. Pena, J. C. Clare, and G. M. Asher, "Doubly fed induction generator using back-to-back PWM converters and its application to variable-speed wind-energy generation," *IEE Proceedings – Electric Power Applications*, vol. 143, no. 3, pp. 231-241, May 1996.

[41] D. W. Novotny and T. A. Lipo, "Vector control and dynamics of AC drives," Oxford University Press, 2000. ISBN-13: 978-0198564393.

[42] L. Xu and Y. Wang, "Dynamic modeling and control of DFIG-based wind turbines under unbalanced network conditions," *IEEE Transactions on Power Syst.*, vol. 22, no. 1, pp. 314-323, Feb. 2007.

[43] J. Hu, Y. He, L. Xu, and B. W. Williams, "Improved control of DFIG systems during network unbalance using PI–R current regulators," *IEEE Transactions on Industrial Electronics*, vol. 56, no. 2, pp. 439-451, Feb. 2009.

[44] D. Xiang, L. Ran, P. J. Tavner and S. Yang, "Control of a doubly-fed induction generator in a wind turbine during grid fault ride-through," *IEEE Transactions on Energy Conversion*, vol. 21, no. 3, pp. 652- 662, 2006.

[45] F. K. A. Lima, A. Luna, P. Rodriguez, E. H. Watanable and F. Blaabjerg, "Rotor voltage dynamics in the doubly-fed induction generator during grid faults," *IEEE Transactions on Power Electronics*, vol. 25, no. 1, pp. 118-130, 2010.

[46] J. Yao, H Li, Y. Liao, and Z. Chen, "An improved control strategy of limiting the DC-link voltage fluctuation for a doubly fed induction wind generator," *IEEE Transactions on Power Electronics*, vol. 23, no. 3, pp. 1205-1213, May 2008.

[47] M. El Moursi, G. Joos, and C. Abbey, "A secondary voltage control strategy for transmission level interconnection of wind generation," *IEEE Transactions Power Electronics*, vol. 23, no. 3, pp. 1178-1190, May 2008.

[48] A. Mullane, G. Lightbody, and R. Yacamini, "Wind-turbine fault ride-through enhancement," *IEEE Transactions on Power Systems*, vol. 20, no. 4, pp. 1929-1937, Nov. 2005.

[49] R. G. de Almeida, J. A. Pecas Lopes, and J. A. L. Barreiros, "Improving power system dynamic behavior through doubly fed induction machines controlled by static converter using fuzzy control," *IEEE Transactions on Power Systems*, vol. 19, no. 4, pp. 1942-1950, Nov. 2004.

[50] M.R. Rathi, N. Mohan, "A novel robust low voltage and fault ride through for wind turbine application operating in weak grids," in *Proc. 31st Annual Conference of IEEE Industrial Electronics Society (IECON 2005)*, November 2005.

[51] N.P. Quang, A. Dittrich, P.N. Lan, "Doubly-fed induction machine as generator in wind power plant nonlinear control algorithms with direct decoupling," in *Proc. IEEE European Conference on Power Electronics and Applications*, Dresden, Germany, Sept. 2005.

[52] V.-T. Phan H.-H. Lee, "Improved predictive current control for unbalanced stand-alone doubly-fed induction generator-based wind power systems," *IET Electric Power Applications*, vol. 5, no. 3, pp. 275–287, 2011.

[53] D. Santos-Martin, J. L. Rodriguez-Amenedo, and S. Arnaltes, "Direct power control applied to doubly fed induction generator under unbalanced grid voltage conditions," *IEEE Transactions on Power Electronics*, vol. 23, no. 5, pp. 2328-2336, Sept. 2008.

[54] D. Santos-Martin, J. L. Rodriguez-Amenedo, and S. Arnaltes, "Providing ride-through capability to a doubly fed induction generator under unbalanced voltage dips," *IEEE Transactions on Power Electronics*, vol. 24, no. 7, pp. 1747-1757, July 2009.

[55] G. Abad, M. A. Rodriguez, G. Iwanski, and J. Poza, "Direct power control of doubly-fed-induction-generator-based wind turbines under unbalanced grid voltage," *IEEE Transactions on Power Electronics*, vol. 25, no. 2, pp. 442-452, Feb. 2010.

[56] L. Jiang, "Wind energy and power system interconnection, control, and operation for high penetration of wind power," Ph.D Dessertaion, Georgia Institute of Technology, Atlanta, Georgia, 2012.

[57] J. Hu, Y. He, Lie Xu, B. Williams, "Improved control of DFIG systems during network unbalance using pi–r current regulators," *IEEE Transactions on Industrial Electronics*, vol. 56, no. 2, pp. 439-451, Feb. 2009.

[58] G. Saccomando and J. Svensson, "Transient operation of grid-connected voltage source converter under unbalanced voltage conditions," in *Proc. IEEE IAS Annual Meeting*, vol. 4, Sep. 2001, pp. 2419–2424.

[59] H. Song and K. Nam, "Dual current control scheme for PWM converter under unbalanced input voltage conditions," *IEEE Transactions on Industrial Electronics*, vol. 46, no. 5, pp. 953–959, Oct. 1999.

[60] T. K. A. Brekken and N. Mohan, "Control of a doubly fed induction wind generator under unbalanced grid voltage conditions," *IEEE Transactions on Energy Conversion*, vol. 22, no. 1, pp. 129–135, Mar. 2007.

[61] J. Liang, W. Qiao, and R. G. Harley, "Feed-forward transient current control for low-voltage ride-through enhancement of DFIG wind turbines," *IEEE Transactions on Energy Conversion*, vol. 25, no. 3, pp. 836-843, September 2010.

[62] Z. Zhang, L. Xu, Y. Zhang, and B. Guan, "Novel rotor-side control scheme for Doubly Fed Induction Generator to ride through grid faults," In *Proc.* 2010 *IEEE Energy Conversion Congress & Exposition (ECCE* 2010*)*, Atlanta, GA, USA, 2010, pp. 3084 - 3090.

APPENDIX

Table 1. The parameters of the DFIG used in this paper.

Symbol	Parameter	Value
P_{nom}	Nominal power	1.5 MW
V_{nom}	Nominal line-line voltage (RMS)	690 V
F_{nom}	Nominal grid frequency	50 Hz
R_s	Stator resistance	2.139 mΩ
L_s	Stator inductance	4.05 mH
R_r	Rotor resistance	2.139 mΩ
L_r	Rotor inductance	4.09 mH
L_m	Mutual inductance	4.00 mH
N_{sr}	Stator to rotor turns ratio	0.369
P	Number of pole pairs	2
τ_s	Stator time constant	1.89 s